

DRAFT

A Volcano Rekindled: The First Year of Renewed Eruption at Mount St. Helens, 2004–2006. Edited by David R. Sherrod, William E. Scott, and Peter H. Stauffer
U.S. Geological Survey Professional Paper 2007-XXXX

Chapter 19. From Dome to Dust: Shallow Crystallization and Fragmentation of Conduit Magma During the 2004–2006 Dome Extrusion of Mount St. Helens, Washington

By Katharine V. Cashman, Carl R. Thornber, and John S. Pallister

Abstract

An unusual feature of the 2004–2006 eruptive activity of Mount St. Helens has been the continuous growth of successive spines that are mantled by thick fault gouge. Fault gouge formation requires, first, solidification of ascending magma within the conduit, then brittle fragmentation and cataclastic flow. We document these processes through observations of field relations, hand samples, and thin section textures. Field observations show that the gouge zone is typically 1–3 m thick and that it includes cataclasite and sometimes breccia in addition to unconsolidated (true) gouge. The gouge contains multiple slickenside sets oriented subparallel to each other and to the striation direction, as well as surface striations parallel to extrusion direction. Hand specimens show both cataclasite and gouge to be composed of a wide size range of broken dome and wall-rock fragments. This grain size heterogeneity is even more pronounced in thin section, where individual samples contain fragments that span more than four orders of magnitude in size (from more than 10 to less than 10^{-3} mm).

Textures preserved within the gouge zone provide evidence of different processes operating in time and space. Most individual fragments are holocrystalline, suggesting that crystallization of the ascending magma preceded gouge formation. Cataclasite samples preserve a wide range of clast sizes; pronounced rounding of many clasts indicates extensive abrasion during transport. Within the gouge, crystals and lava fragments adjacent to finely comminuted shear zones (slickensides) are shattered into small angular fragments and either preserved in place, with little disruption, or incorporated into shear trains to create a well-developed foliation. Together, evidence of initial grain shattering followed by shear, grinding and wear, suggests extensive transport distances (large strains). Textural transitions are often abrupt, indicating extreme shear localization during transport. Comparison of groundmass textures from dome lavas and fault gouge further suggests that brittle fracture was probably confined to the upper 400–500 m of the conduit. Observed magma extrusion (ascent) rates of ~ 7 m/d (8×10^{-5} m/s) permit several weeks for magma ascent from ~ 1000 m (where groundmass crystallization becomes important) to ~ 500 m, where solidification nears completion. Brittle fracture, cataclastic flow, and

shear localization (slickenside formation) probably dominated in the upper 500 m of the conduit.

Comparison of eruptive conditions during the current activity at Mount St. Helens with those of other spine-forming eruptions suggests that magma ascent rates of $\sim 10^{-4}$ m/s allow sufficient degassing and crystallization within the conduit to form large volcanic spines of intermediate (andesite to dacite) composition. Solidification deep within the conduit, in turn, requires transport of the solid plug over long distances (hundreds of meters); resultant large strains are responsible for extensive brittle breakage and development of thick gouge zones. Moreover, similarities between gouge textures and those of ash emitted by explosions from spine margins indicate that fault gouge is the origin for the ash. As the comminution and generation of ash-sized particles was clearly a multi-step process, this observation suggests that fragmentation preceded, rather than accompanied, these explosions.

Introduction

The 2004–present eruption of Mount St. Helens has been characterized by steady lava effusion in the form of a succession of smooth-surfaced dacitic spines (Scott and others, this volume, chap. 1) that are remarkable for the striated fault gouge that forms a carapace on each of the seven spines erupted between October 2004 and February 2006. This fault gouge is unusually well preserved and well sampled, thanks to helicopter dredging operations (see Pallister and others, this volume, chap. 30). Additional geophysical constraints on dome extrusion include photogrammetry (Schilling and others, this volume, chap. 8), thermal observations (Schneider and others, this volume, chap. 17) and seismic observations (Moran and others, this volume, chap. 2). Notable in these observations is the remarkable steadiness of both the extrusion and accompanying ‘drumbeat’ earthquakes, all of which appear to originate at depths < 1 km directly below the growing dome (Moran and others, this volume, chap. 2) and are interpreted to record steady stick-slip behavior of the ascending magma plug (Iverson and others, in review; Iverson, this volume, chap. 21).

Individual outcrops document an abrupt transition from competent flow banded dacite to a zone of breccia and cataclasite to finely comminuted and variably consolidated gouge. In this paper we use field, hand specimen, and thin section observations of these cataclastic dome facies to constrain some of the

physical processes related to dome extrusion and gouge formation. Analysis of observations over this range in scale allows us to (1) describe progressive fragmentation of the solid dome rock to fine-grained fault gouge, (2) trace decompression/crystallization paths within the conduit, and (3) provide depth constraints on both solidification and onset of brittle deformation. We then link processes of fragmentation and gouge formation to relative rates of ascent (shear), degassing, and crystallization. This linkage is important both for recognizing conditions that may lead to changes in the emplacement conditions of the current dome at Mount St. Helens and for generalizing observations at Mount St. Helens to other recent effusive eruptions of intermediate composition magma. In addition, the spectacular preservation of fault textures allows us both to extend analysis of tectonic gouge formation to volcanic environments and to compare brittle deformation processes in highly crystalline dacite with those of tuffites in obsidian flows. Finally, the similarity of clasts preserved within the gouge to those found within ash from dome explosions (Rowe and others, this volume, chap. 29) allows us to speculate on the nature of explosions that have accompanied dome formation.

Background

As detailed descriptions of lava dome emplacement are provided in other papers in this volume (Scott and others, chap. 1; Schilling and others, chap. 8; Vallance and others, chap. 9), here we briefly review only the elements of the dome emplacement history that are directly relevant to the conditions of gouge formation. We then provide an overview of spine formation at other volcanoes, with a particular emphasis on both observations of spine emplacement and eruption conditions that produced these features. Finally, we discuss observational and experimental constraints on decompression-driven crystallization required to form spines.

2004–2006 activity at Mount St. Helens

After about three weeks of precursory seismic unrest and phreatic explosions in late September and early October of 2004, a dacite lava spine emerged within the central crater of Mount St. Helens, to the south of the 1980–1986 lava dome. Extrusion has been continuous

since November 2004, with emplacement and partial to complete disintegration of seven individual spines. Extrusion rates were highest, about 6 m³/s, during the first month of the eruption. Extrusion rates have since dropped to 1–2 m³/s. Linear rates of spine emergence from the vent have also been constant at 3–6 m/day (3.5–7×10⁻⁵ m/s) except during the early stages of extrusion, when rates were about twice as fast. Extrusion has been accompanied by only two major explosions—one on January 16, 2005 and one on March 8, 2005. Ash produced by those explosions is described by Rowe and others (this volume, chap. 29).

Lava dome emplacement and morphology

Howel Williams (1932) presented the first comprehensive description of volcanic dome emplacement. He used the term *dome* to describe viscous lava protrusions that could be subdivided into (1) *plug domes* (spines), (2) *endogenous domes* that grow by expansion from within and (3) *exogenous domes* built by surface effusion, usually from a central summit crater. He noted that effusion rate (*Q*) provided the strongest control on growth style, with the lowest effusion rate leading to plug dome (spine) formation. As type example for plug dome behavior he used the famous spine extruded from Mont Pelée, Martinique, in 1903. This massive spine reached a maximum height of >300 m, grew as rapidly as 25 meters in a day (2.9×10⁻⁴ m/s), and was continually disrupted by both collapse and explosions. It was described by Jaggar (1904) as "... a most extraordinary monolith, shaped like the dorsal fin of a shark, with a steep and almost overhanging escarpment on the east, while the western aspect of the spine was curved and smooth in profile. The field glass showed jagged surfaces on the steeper eastern side, and long smooth striated slopes on the western" (fig. 1). These smooth striated slopes also preserved slickensides and breccias produced by differential movement of already solid lava. Lacroix (1904) noted both vertical striations parallel to the extrusion direction and horizontal ridges indicating "successive stages in its upheaval" (Williams, 1932).

Recent eruptions at Mount St. Helens (Wash.), Unzen (Japan), and Soufrière Hills (Montserrat) confirm and extend these early concepts. Dome growth at Mount St. Helens from 1980 to 1986 had both exogenous and endogenous phases and erupted a total volume of 0.077 km³ of dacite (62.5–63.5 percent SiO₂) magma (Swanson and Holcomb 1990). Exogenous growth of individual flow lobes was the dominant dome growth mechanism through 1981, with lobes emplaced at rates

of 9–24 m³/s over time periods of less than a week. Exogenous dome lobes were also emplaced from March 1984 until October 1986, although accompanying endogenous growth became increasingly important over this time period (Fink and others, 1990). Times of anomalous activity included (1) March 1982, when a protracted effusive event (24 days at an average rate of 1.6 m³/s) was preceded by deep seismicity and a vulcanian explosion; (2) February 1983–February 1984, when effusion was continuous at a rate of 0.7 m³/s (approximately equivalent to the long-term magma supply rate from October 1980 to October 1981) and dome growth was primarily endogenous; and (3) May 1985, when effusion lasted 17 days (at an average rate of 2.9 m³/s). Only two spines were emplaced during this time period, one in February 1983, during the period of continuous endogenous growth, and the other at the end of the protracted dome growth episode in May 1985 (again, largely endogenous). Magma batches feeding individual exogenous dome lobes ascended at 0.1–1 m/s (Chadwick and others, 1988; Endo and others, 1990; Geschwind and Rutherford, 1995), corresponding to decompression rates of ~0.0025–0.025 MPa/s. As effusion rates were 10–20 times lower during 1983, we infer that ascent rates during periods of continuous dome

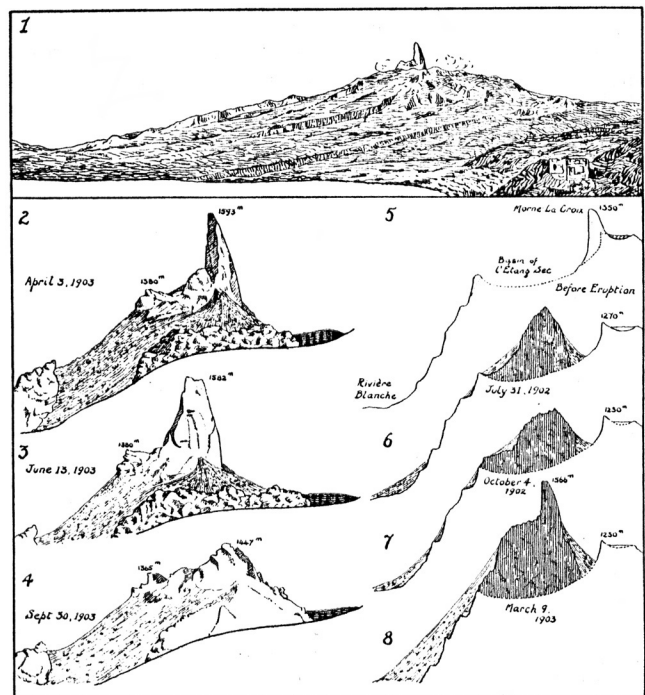


Figure 1. Sketches showing evolution of the great spine of Mont Pelée, Martinique, erupted in 1903. Note difference between smooth curved fault surface and rough near-vertical face. From Williams (1932).

growth were correspondingly lower (that is, at least by a factor of 2–5), with magma ascent rates for spine production even lower (probably $<10^{-3}$ m/s).

Links between eruption rate and dome morphology can be further constrained by examining two other eruptions of slightly different bulk composition. Unzen volcano, active from 1990–1995, constructed a 0.2 km³ dome of dacitic composition (64.5–66 wt percent SiO₂). Initial effusion (Q) at ~ 1 m³/s produced a spine. Shortly thereafter a rapid increase in Q to ~ 5 m³/s triggered a succession of pyroclastic flows accompanied by tremor spurts and two vulcanian eruptions (Nakada and Fujii, 1993; Nakada and others, 1995; 1999; Nakada and Motomura 1999). After this time the dome grew nearly continuously, with exogenous growth dominating for higher effusion rates (> 4 m³/s) and endogenous growth dominant when effusion rates were low (< 1 m³/s). Magma ascent rates are estimated at 13–40 m/d ($1\text{--}5\times 10^{-4}$ m/s; Nakada and others, 1995), more than an order of magnitude lower than during the time period of continuous magma ascent at Mount St. Helens in 1983. Effusion rates declined gradually until the end of the eruption, which was marked by the emergence of a spine from the endogenous dome (Nakada and others, 1999).

Soufrière Hills volcano, Montserrat, intermittently active since 1995, has also shown a close correspondence between the rate of lava effusion and dome morphology. By 1999 it had produced almost 0.3 km³ of silicic andesite (57–61.5 wt percent SiO₂), about two thirds of which traveled as pumiceous and dense pyroclastic flows into valleys around the volcano. Here low effusion rates ($Q \sim 0.5\text{--}2$ m³/s) produced a range of spine and whaleback features, most of which grew in a matter of days. Moderate effusion rates ($Q \sim 2\text{--}7$ m³/s) gave rise to shear lobes that were active for days to weeks to months. High effusion rates ($Q \sim 7\text{--}9$ m³/s) produced pancake-shaped lava lobes with flat tops and scoriaceous surfaces; $Q > 9$ m³/s led to vulcanian explosions (Watts and others, 2002). Of particular interest are features that bear close similarity to current activity at Mount St. Helens, specifically vertical spines and megaspines that characterized magma emplacement at low volumetric effusion rates (< 2 m³/s; Watts and others, 2002).

Together these case studies present a consistent story of spine growth under conditions of slow magma effusion (typically $Q < 1\text{--}2$ m³/s). Descriptions of both smooth and striated spine surfaces are common; Watts and others (2002) inferred that these characteristic curved surfaces were controlled by shear faults (for example, Donnadieu and Merle, 1998) in magma made highly viscous by late-stage decompression-driven crystallization. In fact, as reviewed above, spine morphology has been generally interpreted to reflect

extrusion of a solid lava plug, which probably solidified more as a consequence of decompression-induced crystallization than of cooling en route to the surface. However, there has been no detailed characterization of these bounding fault surfaces, comparison of striated surfaces with tectonic fault textures, or attempt to use either fault surface characteristics or crystallization textures to constrain the conditions of magma ascent and decompression that create these striking volcanic features.

The importance of decompression-driven crystallization

In the early part of the 20th century there was great debate about the solidification mechanism that could generate the large Mont Pelée spine. Lacroix (1904) favored rapid cooling on exit from the vent. Gilbert (1904), on the other hand, suggested that solidification of the spine might result from “escape of gases and formation of bubbles” rather than loss of heat by conduction. This concept was extended by Shepherd and Merwin (1927), who argued that gas pressures required to support the spine (~ 10 MPa) resulted from crystallization; they went on to suggest that these high gas pressures also caused the explosive generation of nuees ardentes that accompanied spine extrusion. Williams (1932) extended this concept to explain late-stage explosions at several other domes, an association that Newhall and Melson (1983) find in most historical eruptions.

Dome growth during the 1980–1986 eruption of Mount St. Helens provided the first quantitative documentation of decompression-driven crystallization in silicic magmas (Cashman, 1992). Decompression-driven crystallization has since been documented during effusive and intermittent explosive phases of numerous recent eruptions (for example, Nakada and others, 1995; Wolf and Eichelberger, 1997; Gardner and others, 1998; Nakada and Motomura, 1999; Hammer and others, 1999, 2000; Cashman and Blundy, 2000; Martel and others, 2000; Sparks and others, 2000; Metrich and others, 2001; Blundy and Cashman, 2005; Cashman and McConnell, 2005) and is generally considered to be the dominant solidification mechanism in slowly ascending hydrous magma of intermediate composition. Petrographic observations show that plagioclase is the most abundant shallow crystallizing phase, a consequence of the profound effect of dissolved H₂O on its stability. Quartz (or some other silica phase) joins the crystallizing assemblage when the quartz-feldspar cotectic is intersected, which typically occurs at low pressures, and rapidly increases the total crystal

abundance. Both the number and mode of plagioclase crystals vary with decompression path (effective undercooling; T_{eff}).

Decompression experiments on H_2O -saturated melts (Geschwind and Rutherford, 1995; Hammer and Rutherford, 2002; Martel and Schmid, 2003; Couch and others, 2003) show that plagioclase number density, size, and morphology are controlled by the rate of decompression and the final pressure of equilibration. The extent of crystallization is dependent on both equilibration pressure and experiment duration (Hammer and Rutherford, 2002; fig. 2). Crystallinity increases as equilibration pressure decreases and with increasing time at a given pressure. At shallow pressures (≤ 25 MPa), extensive crystallization requires time scales of several weeks. Crystal nucleation rates are also highest at pressures between 25 and 10 MPa, although nucleation diminishes in importance at very shallow pressures owing to the high viscosity of silicic melts with low H_2O (Hess and Dingwell, 1996). Extensive co-precipitation of quartz and feldspar appears to require equilibration at very low pressures (5–10 MPa).

An additional consequence of extensive late-stage decompression-driven crystallization is the release of latent heat. Evidence of late-stage heating in slowly erupted dome lavas includes both Ti-zoning of magnetite, which increases calculated Fe-Ti oxide temperatures, and reverse zoning of orthopyroxene

(Devine and others, 2003; Pallister and others, 2005). These signs of heating have commonly been interpreted as evidence of basaltic input at depth (for example, Devine and others, 2003). However, a recent study of samples erupted from Mount St. Helens in the early 1980s shows a strong correlation between late-stage heating and shallow crystallization, suggesting instead that this is a signature of shallow release of latent heat (Blundy and others, 2006). As numerical models of conduit flow dynamics show that even small changes in magma temperature have a large effect on magma discharge rate and eruptive behavior (Melnik and Sparks, 2005), localized crystallization-related heating may be an important component of shallow eruption dynamics.

In summary, the morphology of extruded spines—their asymmetric shape, smooth fault-bounded surfaces, and often imposing height—is controlled by effusion conditions: to form these features, magma ascent must be sufficiently slow to allow near-complete volatile exsolution, degassing, and groundmass crystallization within the conduit. Outstanding questions include the relative timing of groundmass crystallization and fault formation, the potential role of latent heating in shear localization, the strain accommodated along these fault surfaces, the deformation mechanisms by which resulting fault gouge may affect plug extrusion, and the relation between observed seismic signals and spine emplacement.

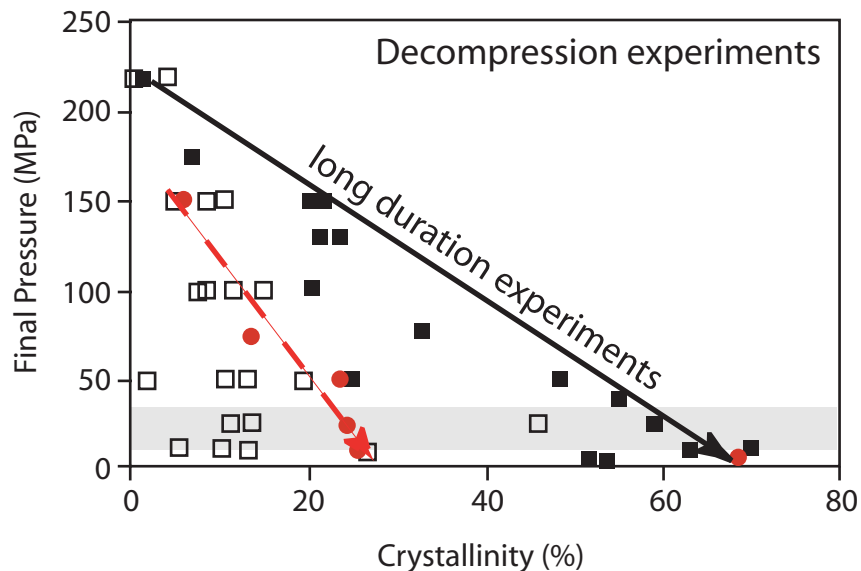


Figure 2. Relative effects of decompression time and equilibration pressure on crystallization of hydrous silicic melts. Squares show single-step decompressions followed by annealing at the final pressure; open squares are short-duration experiments (< 30 hours); filled squares are long-duration experiments (168–931 hours). Gray circles show results of multi-step decompression at constant rate of 1.2 MPa/hr. Data from Hammer and Rutherford (2002). Arrow shows equilibrium decompression-crystallization trend.

Methods

Field observations and digital photography of the 2004–2006 Mount St. Helens dome made during two short ground-based sampling missions and numerous close-in helicopter flights provide an outcrop-scale context for describing the character and origin of the gouge. Because of safety concerns, sampling of the dome and the dome carapace were accomplished primarily by helicopter dredging (Pallister and others, this volume, chap. 30). Although this remote technique did not allow detailed mapping of field relations, it did allow access to steep and unstable parts of the spines that could not have been reached on foot. The source areas for debris and talus samples are, in most cases, well constrained by field documentation. Moreover, both photographic and seismic records document the locations and timing of specific rockfall events sampled. Finally, two days of field work in the summer of 2006 confirmed field relations inferred from remote techniques (Pallister and others, this volume, chap. 30). Distinct differences in sample lithology can be correlated with dome rock facies observed in the walls of scree slopes on the dome flanks. A complete catalogue of sample information, including locations, brief descriptions, and bulk chemistry, is provided by Thornber and others (in prep.).

All dome samples have been described and curated at the Cascades Volcano Observatory (Thornber and others, in prep.). Samples of unconsolidated fault gouge (SH303 and SH307) were processed in the Cascades Volcano Observatory Sediment Laboratory. Samples were dry sieved to 63 μm ; size fractions <63 μm were analyzed using a Micrometrics Sedigraph III particle size analyzer. Both dome lava and fault gouge have also been characterized using petrographic analysis. Whole thin sections were scanned at high resolution for general textural characterization and quantitative analysis of plagioclase phenocryst and microphenocryst textures (that is, crystals >30 μm in diameter). Microscopic evaluation of sample textures was accomplished using a JSM-6300V scanning electron microscope (SEM) at the University of Oregon. Thin sections were imaged in backscattered electron (BSE) mode using 10 kV accelerating voltage and 5 nA beam current. Both scanned and BSE digital images were processed and analyzed using Adobe Photoshop and ImageJ 1.34s (NIH Image for Mac OS X) software. Most techniques used are similar to those described elsewhere (for example, Cashman and McConnell, 2005). However, we also experimented with ways of analyzing the size distribution of clasts in the cataclastite for comparison

with sieve data. Analysis of larger (>30 μm) dome fragments was performed on low magnification (20 \times) BSE images. Gray-scale thresholding of individual clasts provided binary images that could be easily processed to allow clast size analysis (fig. 3). All image analysis data were then analyzed using Microsoft Excel.

Results

Here we document processes related to spine extrusion. As the observational record of spine extrusion

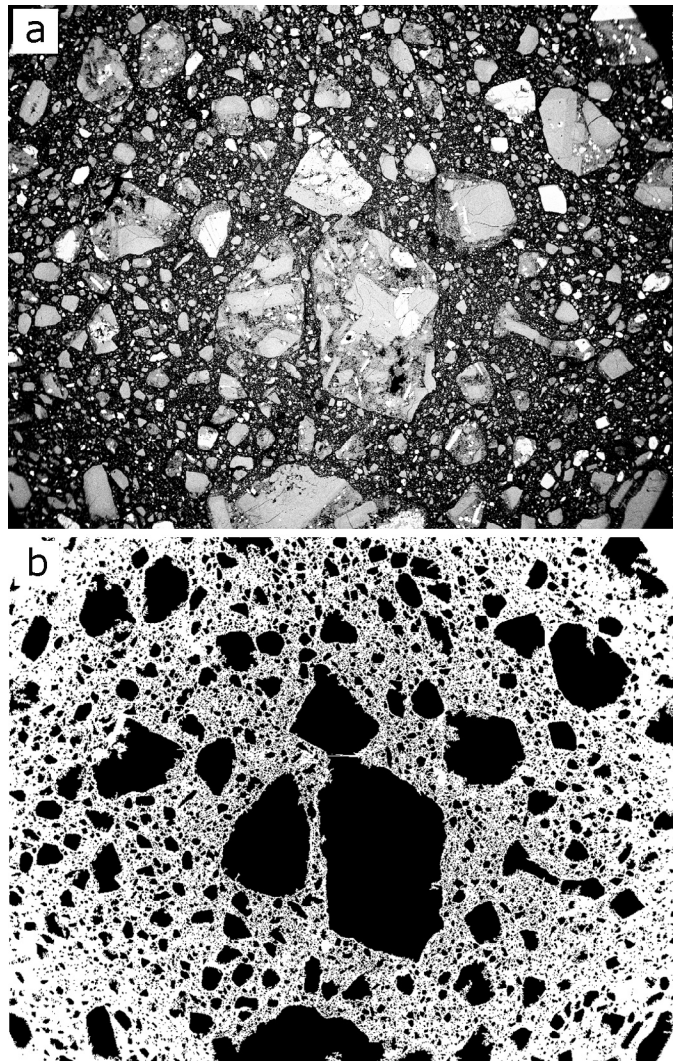


Figure 3. Examples from gouge sample SH326_2a illustrating the image processing technique used to acquire grain size data on cataclastic samples. Apparent circular concentration of very fine particles is an artifact of the image acquisition technique; for this reason only larger particles are used in final analysis. Images are 6.1 mm across. *A*, Backscattered electron image. *B*, Processed binary image.

is unique in the level of detail permitted by the novel sampling techniques, our primary goal is to provide comprehensive descriptions of textures produced as competent dacite lava is transformed into ultracataclastic fault gouge. We begin by reviewing details of field observations, followed by hand-specimen descriptions and thin section observations. To describe the textural characteristics of fault rock samples we follow Snoke and others (1998) in using the nomenclature convention of Sibson (1977) as modified by Scholz (1990), where *gouge* refers to noncohesive material with visible fragments constituting <30 percent (by volume) of the rock mass, in contrast to fault *breccia* that has >30 percent visible fragments. Although this convention would apply the term *cataclasite* to all cohesive brittle

fault rocks, we distinguish cohesive breccia from cataclasite on the basis of apparent clast vs. matrix support. Moreover, for simplicity we refer simply to the *gouge zone* when discussing the entire complex of cataclastic material overlying massive dome dacite.

The view from the field

The gouge carapace was first observed on November 7, 2004, on the surface of spine 3. At that time a large lava spine (300–400 m N–S by 50–150 m E–W) had been thrust to a height of ~100 m above the surface of the already-uplifted glacier in the southeastern quadrant of the crater (figs. 4A, 4B). On the west face of the spine, a slope of gouge was exposed above a basal apron of

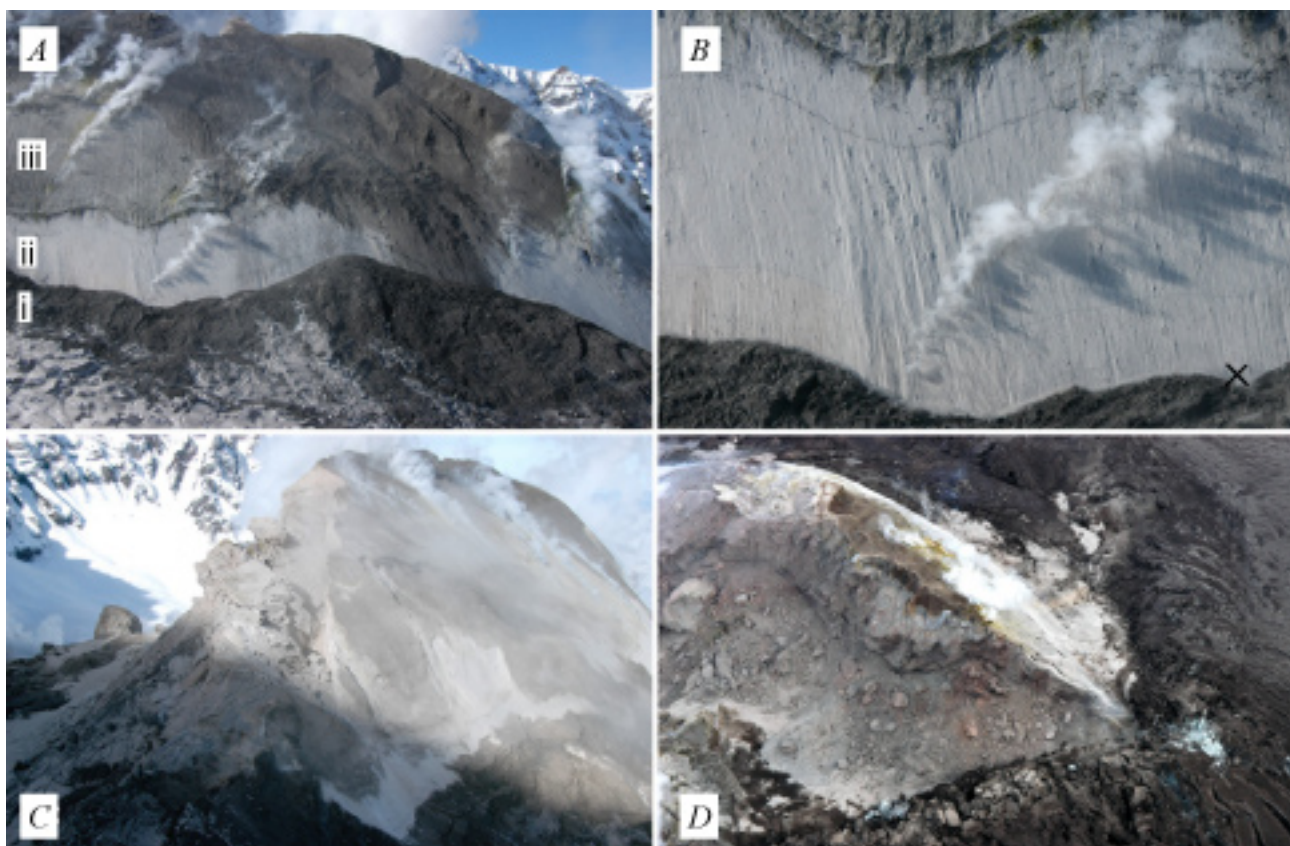


Figure 4. Photographs of spine 3, taken on November 4, 2004. *A*, West-looking view showing, from the base upward: (i) an apron of sandy debris, snow, and glacial ice; (ii) 10–15-m-high wall of white slickenside-bearing gouge with “bathtub rings” that mark former contact levels between gouge surface and debris apron; (iii) dark tan (weathered) gouge or cataclasite with steeply dipping erosional furrows. Blocky outcrops (uppermost spine rough-weathering area near center-frame) are uplifted material from the debris apron. Steam is venting from fractures in gouge carapace. *B*, Close-up photograph of gouge outcrop showing slickensides and “bathtub” rings that parallel contact between gouge and debris apron. Note shadows on the downslope sides of rock fragments within the gouge that suggest up and westward movement of the spine relative to the debris fan. Sample SH303-1 collected from the white powdery gouge at site marked by X, about 1 m above the debris apron 10 m north (right) of the prominent steam vent. *C*, Oblique aerial photograph of the southeast collapsed terminus of spine 3, showing blocky outcrops of dense dacite of the spine interior. View north-northwest. *D*, Photograph of southwest face and south terminus of spine 3 with dark (ash covered) “bulldozed” glacier on right. White gouge carapace is visible above the blocky interior of the collapsing southwest face; powdery gouge eroded from the carapace has been deposited on the debris apron on the east flank of the spine. View northeast.

wet sandy debris containing angular lava blocks. The lower 10–20 m of the exposed east face was composed of gouge that displayed prominent striations plunging steeply west (parallel to the 45° slope of the spine) in exposures along the southeast face and more northerly along the northeast face. Here a resistant surface layer was underlain by ≤ 1 m of white powdery gouge (sample SH303) that was only slightly warm to the touch ($\sim 30^\circ\text{C}$), dry, and friable. Sparse rock fragments within the gouge accumulated fine-grained material on their downslope sides, producing features akin to pressure shadows (Pabst, 1931) with a preserved sense of shear

that was consistent with uplift of the spine core relative to marginal rocks (fig. 4B). Several curvilinear bands of discolored gouge and trails of embedded lithic fragments (“bathtub rings,” figs. 4A, 4B) paralleled the contact between the gouge and the debris apron at the base of the spine, recording earlier positions of this basal contact that shifted upward with growth. Disintegration of the south face of spine 3 (figs. 4C, 4D) allowed sampling of the (still hot) spine interior by helicopter dredging. The dominant rock type is dense hornblende-hypersthene-plagioclase-phyric dacite with a microcrystalline groundmass (SH304; Pallister and others, this volume, chap. 30).



Figure 5. Features of the new lava dome. *A*, Oblique aerial photograph of crater and 2004–2005 lava dome taken from the northwest on June 29, 2005. Spine 3 in shadow on left; spine 4 in center (highly fractured and altered); and spine 5 on right, with white striated gouge carapace on north and west flanks, collapse scar on northwest face, and sharp, arcuate contact between hot powdery gouge and talus marking periphery of the vent. Crevassed and brown, ash-covered Crater Glacier surrounds dome. The following three photos were taken on January 14, 2005. *B*, Striated surface of spine 4; direction of transport is from lower right to upper left. Orange box on instrument package at center of frame is 1 m long. *C*, Contacts between gouge (gray weathered surface lacking distinct striations), underlying cataclastic breccia, and dense dacite exposed on collapsed south face of spine 4. Note flow foliation in lower right of photograph and in some outcrops immediately below gouge. Dacite lava is overlain abruptly by pink to yellow consolidated gouge, which in turn is mantled by powdery white to gray gouge. Preserved thickness of gouge zone above contact is 1–2 m, although original thickness was greater. *D*, Parallel striations on surface of spine 4; transport direction from lower left to upper right. Surface striations mark penetrative fabric that creates planar shear lamination of the cataclasite. Block of dacite collected from interior of spine 4 nearby is flow foliated and displays a strong lineation of elongate amphiboles.

The detailed descriptions of spine 3 provided above can be generalized to all other spines. A narrow band of mantling gouge typically forms an intact annulus at the vent margin (fig. 5A). Thermal data from a Forward-Looking Infrared Radiometer (FLIR) indicate temperatures of 100–200°C at this margin but show that the gouge surface cools to near ambient temperatures after about 10 m of uplift. That temperatures typically remain high in the spine interior (within a few meters of the surface) is indicated by FLIR temperature maxima of 730°C (Schneider and others, this volume, chap. 17). Throughout the eruption, the thickness of the gouge zone has ranged from 1 to 3 m, always with surface striations oriented parallel to transport (fig. 5B). Most commonly, dense flow-banded dacite is abruptly overlain by 1–2 m of reddish cataclasite, which is, in turn, overlain by poorly consolidated white to tan powdery gouge (fig. 5C). Less frequent are examples of foliated gouge with parallel striations on the surface that form a penetrative shear foliation (fig. 5D). Samples of foliated gouge show multiple subparallel slickensides that indicate slight variations in slip direction at different depths. In some outcrops, a capping resistant (and striated) surface layer protects the unconsolidated gouge, at times posing challenges to sampling efforts: on one occasion a 75-kg dredge was dragged along the surface of spine 4 without penetrating this surface layer. Bulk chemical analyses of gouge samples show that early gouge included a substantial fraction of older material from the conduit margin, whereas later gouge samples are mostly juvenile dacite (Rowe and others, this volume, chap. 29).

An unusual, well-exposed section of the lava-to-gouge boundary within a graben that had formed in spine 4 was photographed in December 2005, more than a year after spine extrusion (fig. 6). Exposed cross sections of the gouge-lava contact showed both breccia and pink (altered) cataclasite separating massive flow-banded dacite from overlying powdery gouge. The abrupt contact between massive dacite and the overlying cataclasite requires this to be an important mechanical boundary. The progression from breccia to gouge was well displayed, with blocks of intact dacite sheared from the underlying lava and progressively fragmented to produce breccia, cataclasite, and gouge. The sense of brittle shear derived from the inclination of shear surfaces within the breccia is consistent with upward transport from the vent. Photographic interpretations were confirmed by field observations in the summer of 2006, which showed the gouge to have formed over a vertical distance of 1–2 m by shear between the upward-thrusting dacite within the conduit and the conduit margins. Reidel shears within the cataclasite provide further evidence of brittle shear failure (Pallister and others, 2006).

Hand samples

Rock samples collected from the talus of the growing 2004–2006 Mount St. Helens dacite dome include both competent dacite (igneous rock) and a variety of fault rocks (cataclasite). Detailed descriptions of all samples can be found in Thornber and others (in prep.).

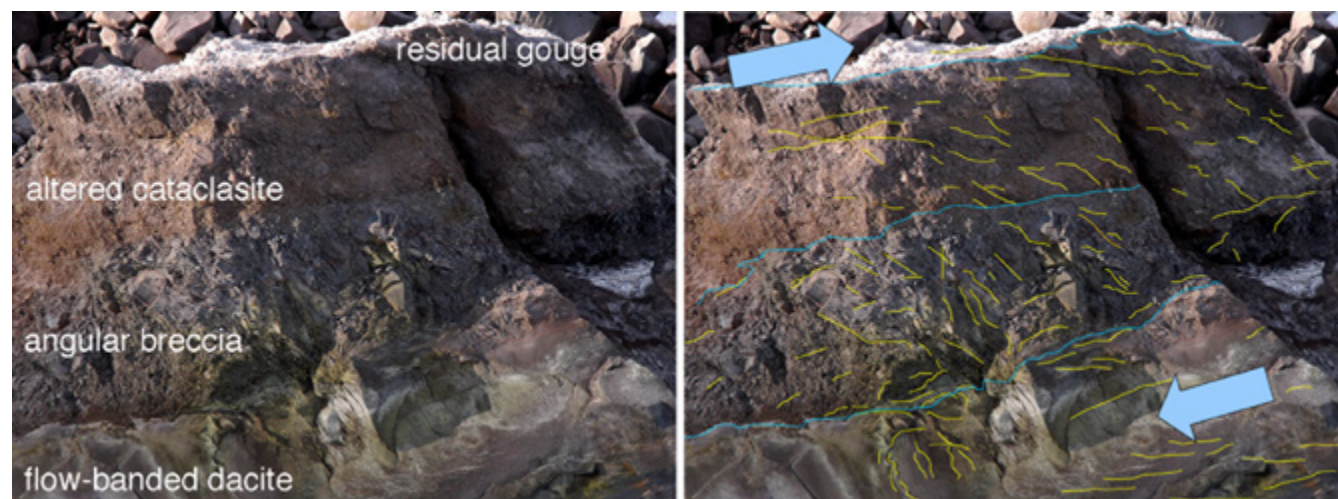


Figure 6. Dome-breccia relations. *A*, Erosional remnant atop spine 4, photographed on December 15, 2005, preserves a breccia interval between massive to flow-banded dacite lava at base of outcrop and a thin surface layer of white powdery gouge. Brittle fractures (Reidel shears) are present in breccia and cataclasite. *B*, Trend lines indicate shear couple with basal dacite moving left (away from vent) relative to upper (external) part of outcrop, consistent with shear between dacite and conduit wall during extrusion. Height of outcrop approximately 3 m.

Here we briefly describe the varieties of pristine dome dacite before describing the range of fault rocks. Dacite samples vary in color from light gray to reddish or pink (a term used in deference to the first unequivocally juvenile samples of “hot pink” dacite SH304). The reddish alteration results from oxidation that is localized around hornblende, oxide, and hypersthene phenocrysts and does not noticeably affect the otherwise igneous fabric of the rocks.

In hand sample, the igneous facies of dome rocks may be broadly classified as (1) dense light-gray (to pink) dacite, (2) flow-banded gray (to pink) dacite and (3) vesicular dark-gray (to pink) dacite. Most samples also contain 1 to 5 vol. percent of coarse-grained hornblende–gabbro norite xenoliths that are similar in abundance and character to those in 1980 to 1986 eruption products (Heliker, 1995). Lithic inclusions of dacite, andesite, and amphibolite are less frequent and typically of smaller size.

Dense light-gray dacite samples dominate the dome talus suite. As these samples are both angular and dense (porosities <10 percent), and as several were dredged from collapse faces of the spines, we infer that they are derived primarily from the dome interior. Flow fabric within the dome facies is not well developed, evidenced only by (1) alignment of acicular hornblende phenocrysts in some samples and (2) entrainment patterns of xenolithic fragments and vesicular pockets around these fragments. Rare *flow-banded dacite* samples have distinctly light-colored or reddish bands (ranging from less than 10 to 20 mm in width) that are subparallel to foliation evident in dense dacite host rock. Bands lack evidence of granular flow or other forms of brittle deformation and instead are characterized by high vesicularity relative to the host rock.

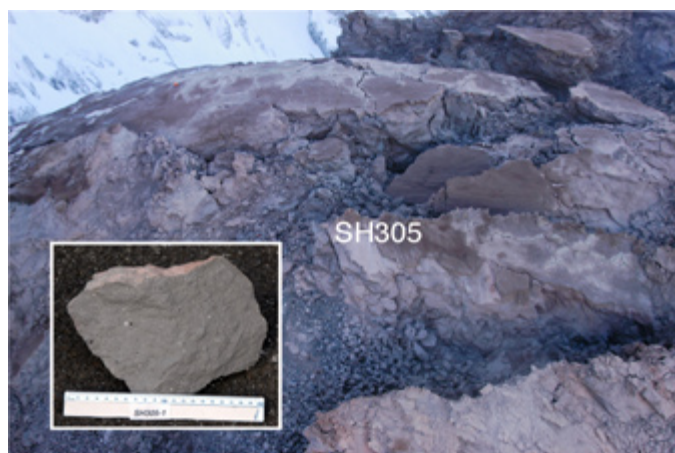


Figure 7. Outcrop and hand specimen photographs of sample SH305, collected January 3, 2005, from spine 3.

Vesicular dacite samples have 25–40 percent porosity and range in color from dark gray to red. In some vesicular samples, igneous flow is evidenced by fanned vesicle distribution patterns and corresponding flow alignment of xenolith fragments and feldspar megacrysts. Proximity of the most vesicular, glassy, and reddish dacite to the outer dome margins is inferred from in-place sampling (SH305-1; fig. 7) and is documented in the exposed cross sections of collapsed spines. Helium-pycnometer measurements of SH305-1 yield a He-accessible porosity of 30.4 percent, nearly identical to the porosity of 30.3 percent determined from the measured bulk density of 1,829 kg/m³ and measured solid density of 2,627 kg/m³. The similarity of the connected and bulk porosity indicates that the pores are fully connected and may therefore allow permeable flow of gas upward along the margin of the conduit. Preliminary permeability measurements on the same samples yields permeabilities of 8–9×10⁻¹³ m², confirming the possible ease of gas flow through the more vesicular dome lavas.

Both abrupt and gradational changes from competent dacite to finely powdered gouge are found within the sample suite. Some fractured and foliated dacite samples reveal a subtle gradation between vesicular dacite and marginal granular gouge. For example, samples from 2–5 m below surface gouge collected in the SH309 dredge along the southern end of spine 4 are somewhat altered and show moderate crushing and compaction associated with post-solidification shearing. Cataclastic rocks are distinguished by visible fragments of dome lava suspended within a finer-grained matrix (figs. 8A, 8B) and range from well consolidated to friable and from coarse to fine grained. Both the size and abundance of macroscopic lava fragments decrease toward the outer surface of fine-grained noncohesive gouge. Friable and foliated gouge from spine 4 (SH313-1) shows pronounced slickensides forming subparallel striations that permeate the loosely consolidated sample (fig. 8C). Powdery fault gouge is light in color and unconsolidated.

Samples in thin section

The petrography and petrology of dacite lava dome samples are described elsewhere (Pallister and others, this volume, chap. 30) and will be reviewed only briefly here. The dacite lava has a uniform bulk composition (65 wt percent SiO₂) and is highly crystalline, with 41–45 percent phenocrysts and microphenocrysts of plagioclase, hypersthene, amphiboles, and Fe-Ti oxides set in a microcrystalline matrix (fig. 9A). Iron-titanium oxide temperatures in early samples are 840–850°C; apparent temperatures increase in later samples in

response to latent heat produced by extensive shallow crystallization (for example, Blundy and others, 2006).

Thin sections provide important insight into fine-scale cataclasis of competent dome lava. An unusual sample (SH324-4a) preserves an abrupt boundary between coherent dome lava and highly fragmented fault gouge. In thin section, the boundary between gouge and coherent lava is marked by thin oxidized bands that lie subparallel to the boundary (fig. 9B). Approximately

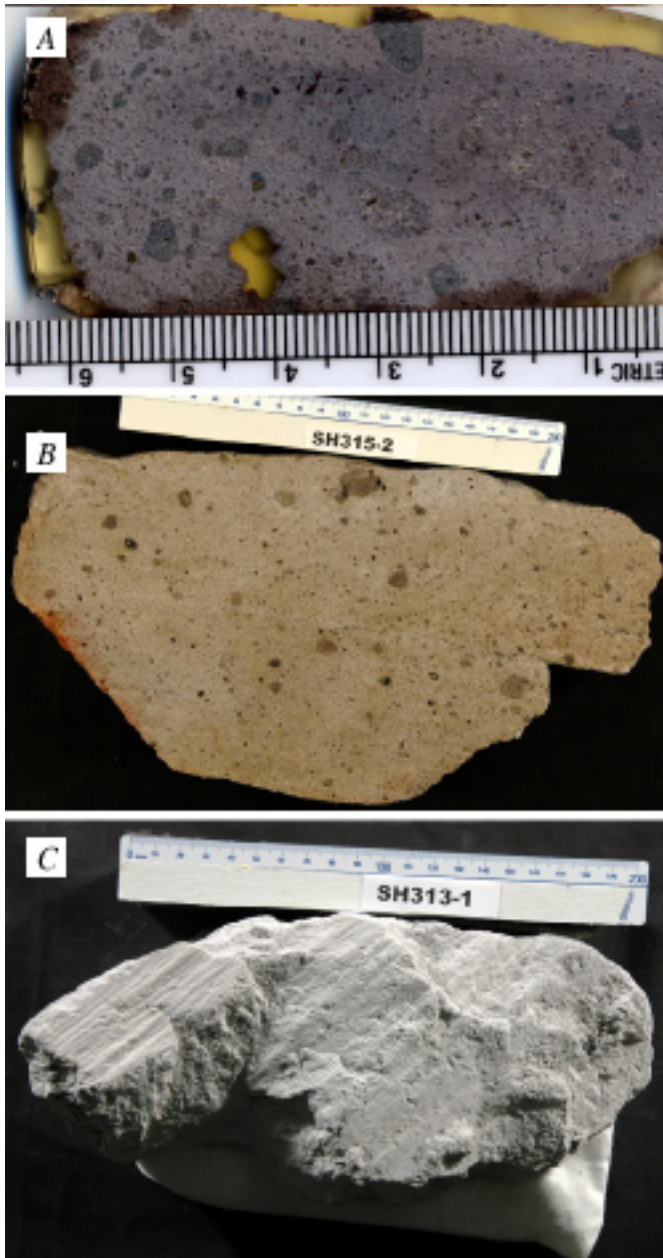


Figure 8. Hand specimen and cut chips showing textural gradation from cataclasite to intensely comminuted fault gouge. *A*, Lithified breccia sample SH326-2a (spine 7); *B*, cataclasite sample SH315-2 (spine 4); *C*, striated gouge sample SH313-1 (spine 4). Scale in centimeters.

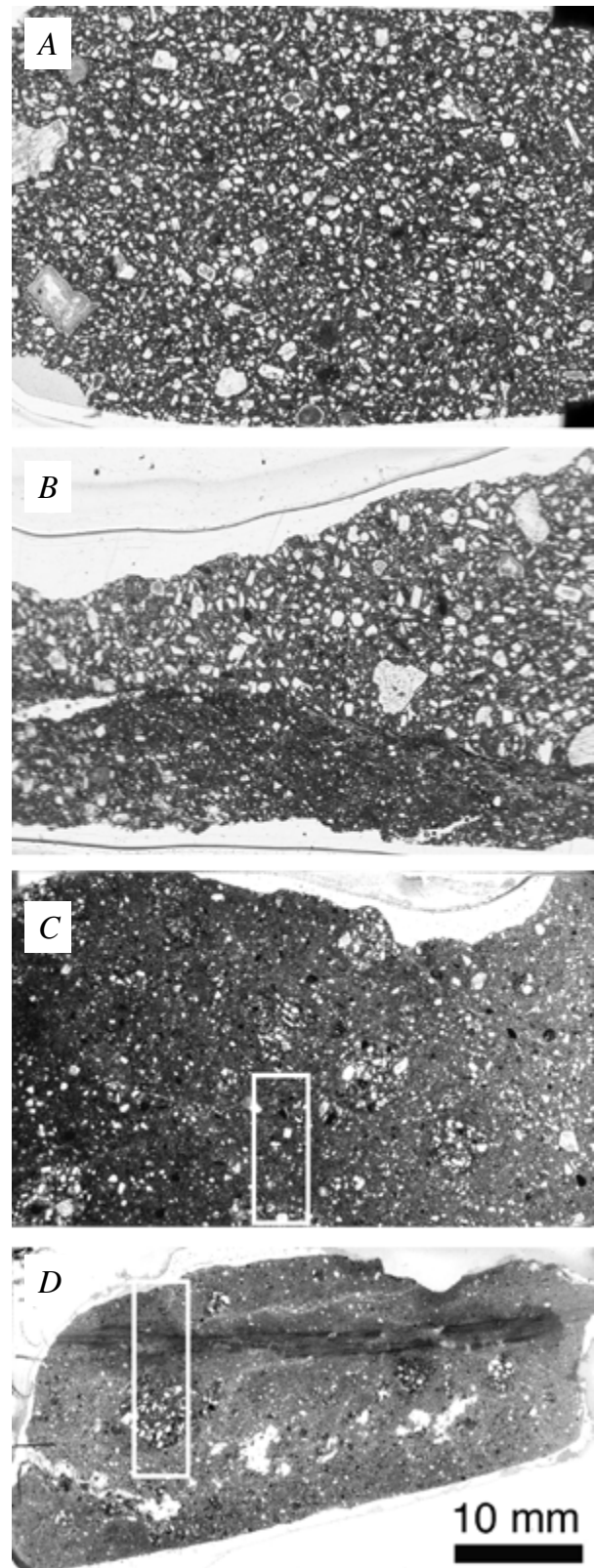


Figure 9. Full thin section scans of samples showing transition from competent dome lava to highly comminuted fault gouge. Scale bar in *D* applies to all four panels. *A*, Sample SH316, from spine 5. *B*, SH324-4a, from spine 7. *C*, SH326-2a, from spine 7; box shows transect illustrated in figure 14A). *D*, SH313-1c, from spine 4; box shows transect illustrated in figure 16A.

parallel to these bands, more subtle variations in matrix density mark a throughgoing shear fabric within the boundary zone. More common are samples of cataclasite that are characterized by rounded fragments of dome lava within a finer grained matrix (SH326; fig. 9C). In thin section, dome fragments typically range from greater than 10 mm to less than 0.1 mm. The matrix comprises primarily shattered phenocrysts, although pieces of holocrystalline groundmass can also be identified. In friable foliated gouge samples with obvious slickensides, the grain size reduction visible in thin section is extreme (SH 313-1; fig. 9D), with typical cataclasite (fig. 9C) cut by an extraordinarily fine-grained foliated shear zone (an ultracataclasite, with grain size $<1\mu\text{m}$). Other thin sections of the same sample show anastomosing branches of foliated ultracataclasite that isolate areas of coarser cataclasite.

BSE observations

Field, hand specimen, and thin section observations of dome and gouge samples offer a picture of competent (and flow-banded) dome lava achieving threshold conditions for wholesale fragmentation, cataclastic flow, and strain localization to accommodate the large strains achieved during spine emplacement. Here we use backscattered electron (BSE) imaging to provide textural evidence for (1) the crystallization history of the dome magma that may have led to fragmentation, (2) fragmentation mechanisms, and (3) evidence for cataclastic flow.

As detailed characterization of phenocryst textures and composition is provided elsewhere in this volume (Pallister and others, chap. 30; Rutherford and Devine, chap. 31; Streck and others, chap. 34), we limit our descriptions of phenocrysts to characteristics that may help to constrain shallow conduit processes. A striking feature of virtually all samples that we have imaged is the presence of some plagioclase phenocrysts ($>100\mu\text{m}$) with irregular margins on one or more growth faces that indicate rapid late-stage rim growth (fig. 10). In contrast, microphenocrysts ($30\text{--}100\mu\text{m}$) are typically euhedral and prismatic. Phenocryst rim growth instabilities range from a few to several tens of microns in width (fig. 10A) and include either multiple (fig. 10B) or single (fig. 10C) growth zones. In some samples, irregular growth protrusions partially entrap small pockets of groundmass glass that are substantially less crystalline and less vesicular than adjacent matrix (fig. 10C). That evidence for rapid rim growth is seen in both early- (fast) and late- (slow) erupted dome lavas and that clean glass is commonly preserved within the growth irregularities suggest that these features reflect relatively fast magma

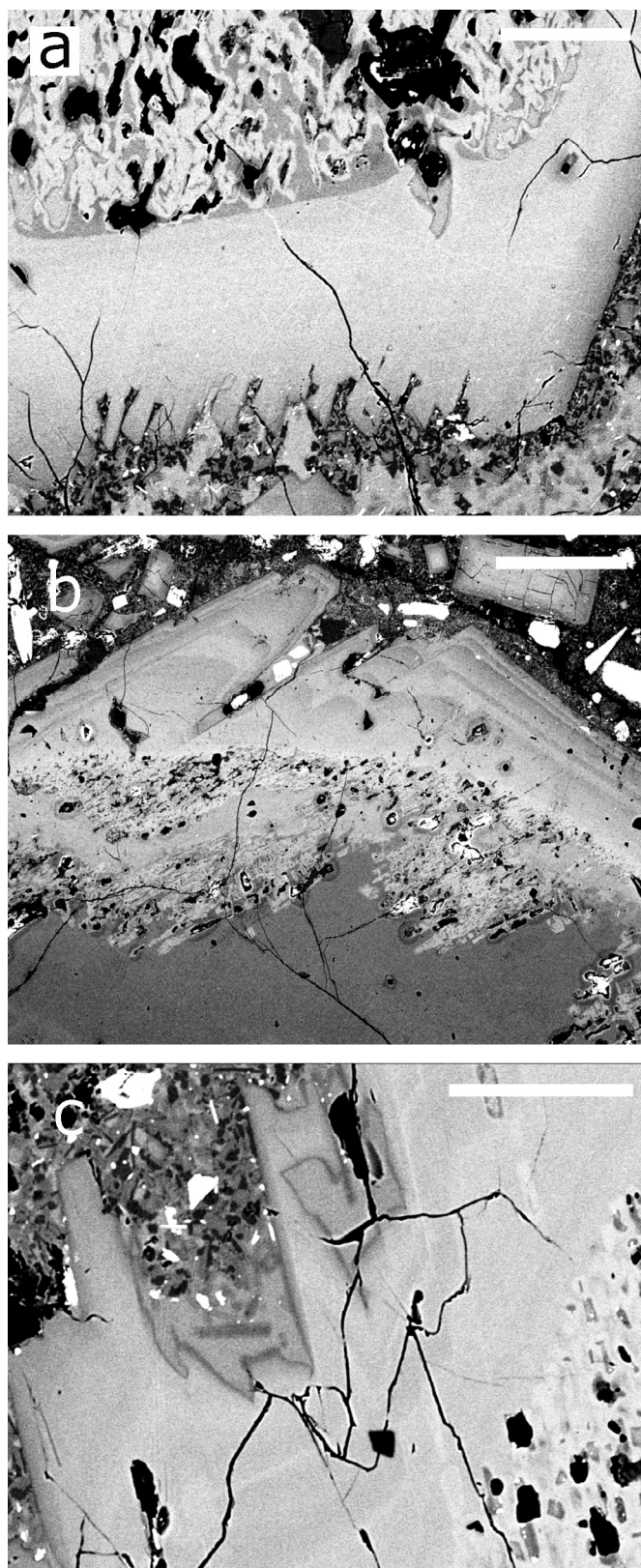


Figure 10. Plagioclase phenocryst textures indicative of rapid growth. *A*, Sample SH316. Scale bar = $50\mu\text{m}$. *B*, Sample SH315-2. Scale bar = $250\mu\text{m}$. *C*, Sample SH309-1. Scale bar = $50\mu\text{m}$.

ascent (and overstepping of the plagioclase liquidus) at deeper levels in the conduit system. That growth irregularities are most common in large (and commonly outsized) phenocrysts suggests that these crystals may have a unique decompression history.

Although the groundmass of all samples is highly crystalline, groundmass textures are quite variable. At one extreme lie juvenile samples collected by dredge in early November 2004 (SH304) that include several unusually glassy clasts. One such clast has only pyroxene and oxides as groundmass phases and preserves ~ 2 wt percent H₂O in the groundmass glass (Pallister and others, this volume, chap. 30). Another sample (SH304-2G3; figs. 11A, 11B) has a groundmass

composed primarily of feldspar microlites (<20 μm in length) with only minor pyroxene, oxides, and quartz. This sample is unusual in having abundant clean glass (~25 percent) and only minimal precipitation of silica phases. Many of the larger plagioclase microlites in this sample have swallowtail terminations that suggest rapid growth (for example, Hammer and Rutherford 2002). High crystal number densities (~ 10⁷/mm³) preserved in this sample would suggest that most of the growth was shallow (< 25 MPa; see compilation in Cashman and McConnell, 2005) in addition to rapid. These pressure estimates are roughly consistent with the ~30 MPa indicated by preserved H₂O contents of some other SH304 clasts, confirming that glassy SH304

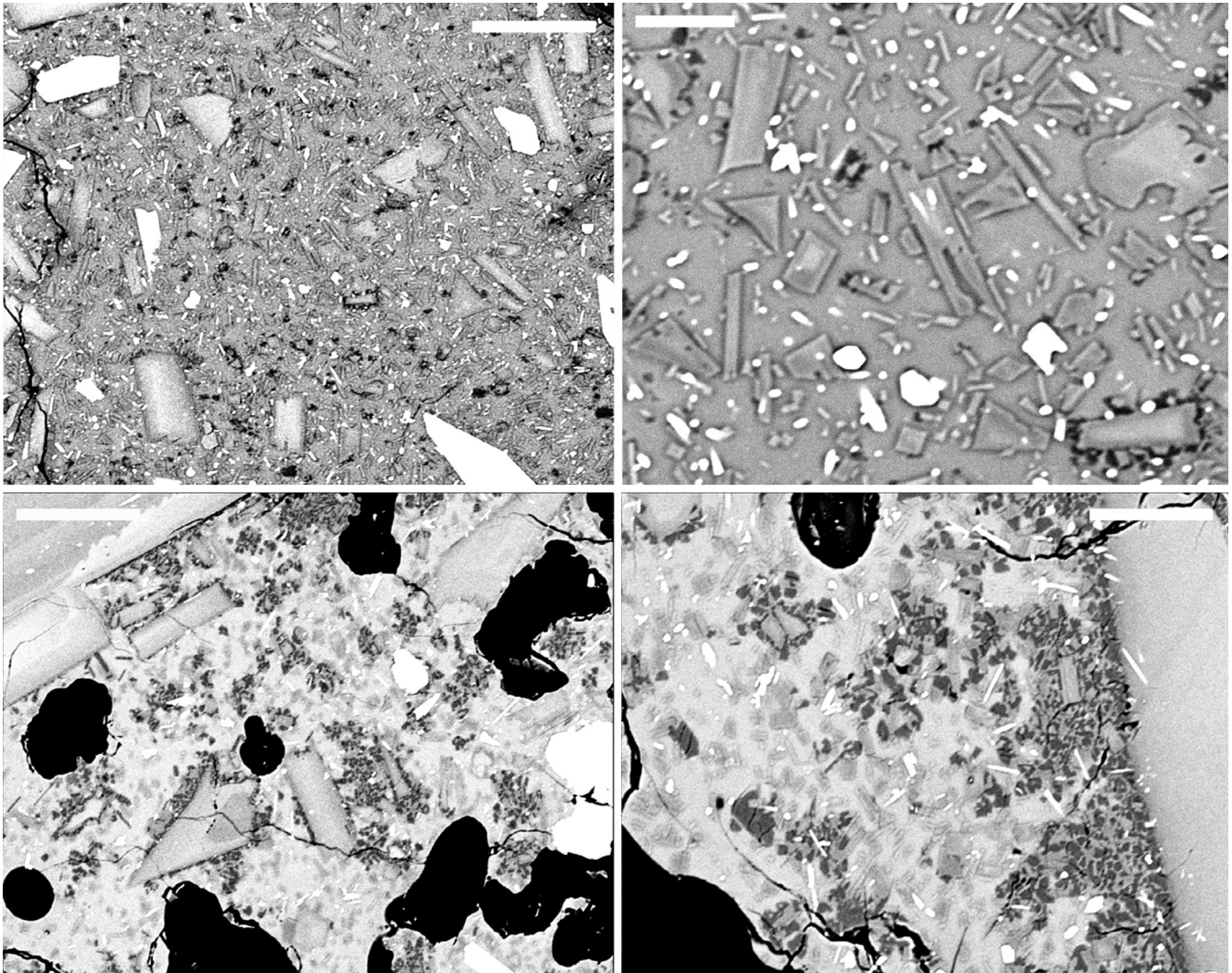


Figure 11. Backscattered electron images of groundmass textures from early-erupted samples (spine 3). *A*, Sample SH304-2G3 showing relatively high glass content and dominance of plagioclase microlites (medium- to light-gray crystals). Scale bar is 50 μm. *B*, Highly magnified view. Scale bar 10 μm. *C*, Sample SH305-1 showing patchy development of cotectic quartz-feldspar intergrowths (blotchy dark-gray regions) with apparent nucleation on phenocryst margins. Scale bar is 50 μm. *D*, Highly magnified view. Scale bar 25 μm.

samples appear to have been quenched at depths ~1 km (for example, Pallister and others, this volume, chap. 30). More typical of early-erupted samples is SH305-1, from spine 3, emplaced in early November 2004 (for example, fig. 7). This sample is distinct from SH304-2G3 in having less-numerous but somewhat more-euhedral plagioclase microlites in a groundmass mottled with 30–40- μm patches of cotectic feldspar and quartz crystallization, intergrowths that commonly nucleate along plagioclase phenocryst and microphenocryst boundaries and then grow into the melt (figs. 11C, 11D). Disequilibrium crystallization is a common feature of natural and experimental melts decompressed slowly to shallow levels (Hammer and Rutherford, 2002; Martel and Schmidt, 2003), the result of delayed quartz nucleation in these highly silicic melts (Cashman and Blundy, 2000; Blundy and Cashman, 2001). Quartz may have nucleated more easily along euhedral crystal margins if a thin, slightly SiO_2 -enriched, boundary layer helped to overcome the activation energy required for

quartz nucleation in the rhyolitic liquid.

By April 2005, the rate of dome extrusion had diminished and groundmass textures are correspondingly more crystalline. Dome dacite sample SH316 (fig. 9A; from spine 5) has a highly crystalline groundmass with abundant plagioclase crystals and patchy cotectic intergrowths of plagioclase and quartz (fig. 12A). Also apparent in the groundmass of SH316 are larger (~50 μm in length) acicular (platy in three dimensions) siliceous crystals that appear to be a form of cristobalite (fig. 12A). Other samples, such as SH309, show abundant tridymite as a groundmass phase (figs. 12B, 12C), a feature that was also observed by Blundy and Cashman (2001) in some samples from the continuous growth phase of the 1983 Mount St. Helens dome. In figure 12B, the long axes of tridymite crystals are locally aligned, recording late-stage deformation.

Backscattered electron imaging also provides a spectacular record of gouge development. As described above, dome dacite samples (fig. 13A) show little sign

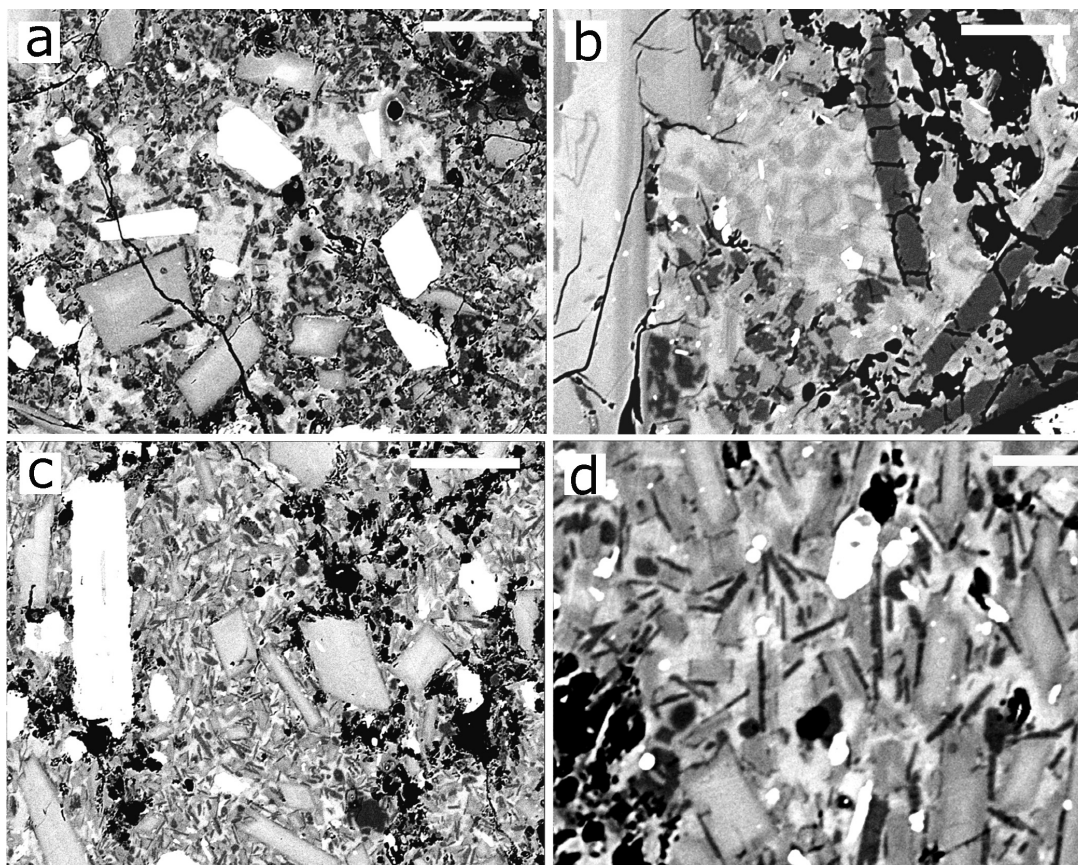


Figure 12. BSE images of groundmass textures from later-erupted samples. *A*, SH 316 (spine 5) showing near-holocrystalline nature of groundmass. Dark-gray phase is quartz, intermediate gray is plagioclase, light gray is quenched glass, and white are mafic phases. Scale bar=50 μm . *B*, High-magnification view of SH316 groundmass showing high number density of plagioclase microlites in remnant clean glass patches. Scale bar=25 μm . *C*, SH309 (spine 4) showing unusual abundance of acicular aligned tridymite crystals in the groundmass. Scale bar=50 μm . *D*, high magnification view of SH309 groundmass showing the intergrowths of plagioclase and tridymite (dark gray) and remnant patches of clean glass. Scale bar=10 μm .

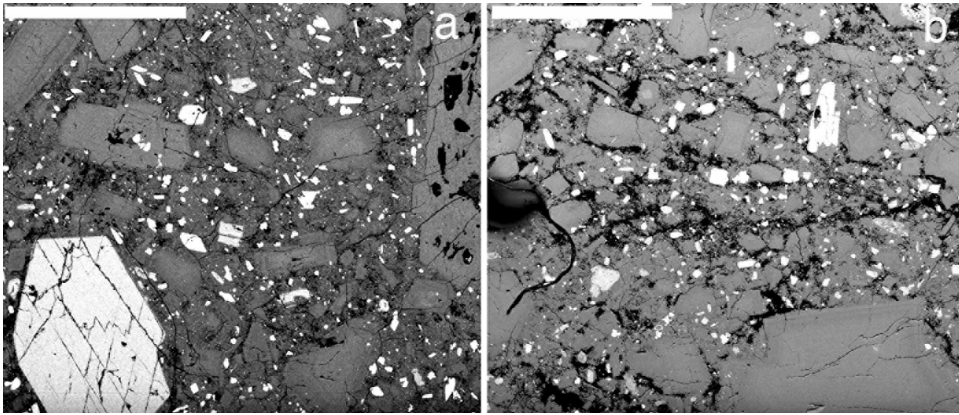


Figure 13. Low-magnification BSE images of two spine 4 samples. Scale bars are 1 mm in both images. *A*, Competent dacite sample SH 308-3A. *B*, partially fragmented sample SH 309-1c. Note extensive fracturing (black areas indicate void space).

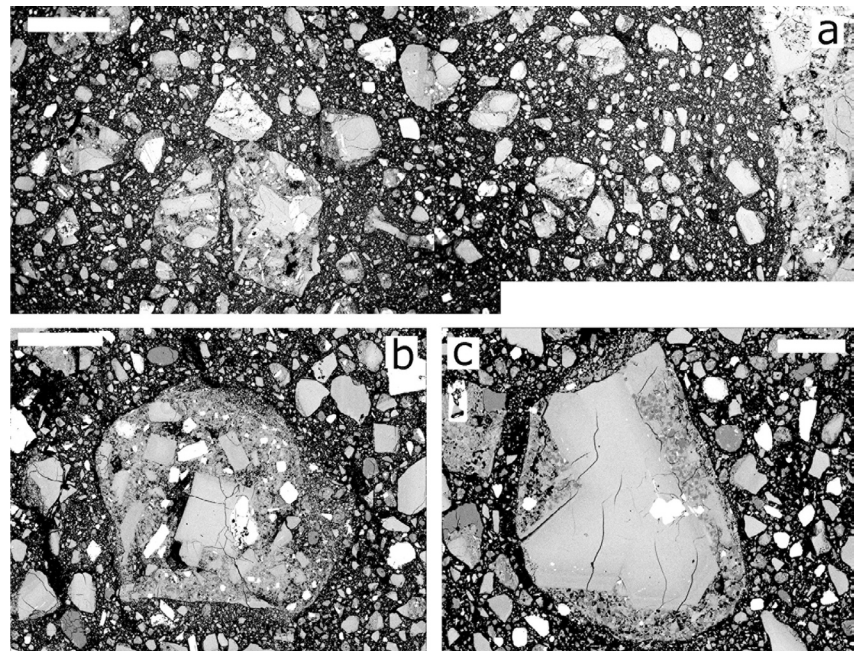
of deformation associated with magma ascent and extrusion, except for some samples with pronounced flow banding. Brittle breakage associated with flow is first manifested as through-going fractures, particularly along phenocryst boundaries (fig. 13B). Cataclasite sample SH326-2a shows much more extensive evidence of crushing. Thin sections illustrate the textural heterogeneity of this sample, with dome lava clasts 10 mm in diameter randomly distributed in a matrix of smaller clasts, individual crystals, and pulverized matrix (fig. 9C). BSE images show that the matrix itself contains a continuous range of fragment sizes, from intact lava clasts greater than 1 mm to tiny fragments smaller than 1 μm (fig. 14A), where crude banding is suggested by regions of higher and lower fragment concentrations.

All samples of both cataclasite and gouge show nearly complete groundmass crystallization; groundmass textures preserved within individual clasts are generally

similar to the more crystalline parts of dome-lava groundmass. Larger fragments within the gouge are typically cored by plagioclase phenocrysts enclosed in holocrystalline (and microvesicular) groundmass (fig. 14B, 14C), although clasts composed entirely of microphenocrysts and microvesicular, holocrystalline groundmass are not uncommon. Often the outer margin of clasts is distinctly rounded and is surrounded by very fine-grained fragments. Both of these features suggest extensive grinding, abrasion, and even rolling during transport.

Samples SH324-4a (fig. 9B) and SH313-1 (fig. 9D) provide a more detailed look at textural transitions from dome lava to gouge to ultracataclasite. In SH324-4a (fig. 15), the pronounced boundary between dome lava and gouge seen in thin section marks an abrupt change from intact holocrystalline igneous groundmass to fragmented and disseminated matrix plus crystals and crystal fragments (fig. 15A). In detail, the boundary is composed

Figure 14. Backscattered electron images of fault gouge textures preserved in sample SH326-2A (spine 7; see fig. 9C for smaller-scale view). *A*, Composite transect illustrating textures characteristic of cataclasite samples. Scale bar=1 mm. *B*, *C*, Typical gouge fragments composed of individual phenocrysts or broken dome matrix surrounded by holocrystalline matrix. Clasts are typically rounded and are surrounded by a halo of finely pulverized material. Scale bar is 250 μm in *B*, 100 μm in *C*.



of thin (~100 μm) slivers of intact holocrystalline groundmass separated by bands of loose crystal and groundmass fragments (fig. 15*B*). In figure 15*B*, the shear-zone margin shows a single plagioclase crystal in the process of being shattered, providing the source of the crystal fragment shear train seen in figure 15*D*. Patterns of fracture may provide a sense of shear, as in figure 15*C*, where conjugate fracture sets propagate through a dome lava fragment containing both crystals and holocrystalline groundmass.

A traverse across foliated gouge sample SH313-1 (figs. 8*C*, 9*D*) shows even more spectacular grain size variation (fig. 16*A*). Much of the thin section is similar to cataclasite sample SH326 (fig. 14), with intact clasts of dome lava suspended in a fine-grained matrix. However, the narrow (≤ 1 mm) fault zone visible in thin section (fig. 9*D*) is, in BSE imagery, composed of alternating bands (~100 μm wide) of fine- (tens of μm s) and extremely fine-grained (<1 μm) material (fig. 16*B*, *C*). By analogy with features observed in SH324-4a (fig. 15), we infer that banding develops by incorporation of shattered crystals (fig. 15*B*) and dome fragments (fig.

16*D*) into adjacent shear zones. Foliation orientations are both parallel and subparallel to the shear-zone orientation, consistent with macroscopic evidence for slight orientation variations among slickensides (fig. 8*C*). Moreover, in some locations along the shear zone, individual fragments of foliated gouge have been broken and rotated (figs. 16*C*, 16*D*). In other locations, the shear zone itself is anastomosing, forming an ultracataclastic zone that varies in both width and complexity (fig. 16*E*). Here, too, the orientation of individual foliated layers within the gouge is subparallel to the shear zone.

Grain size measurements

Sieve data for two powdery gouge samples—SH303-1 collected on November 11, 2004, from spine 3 and SH307-1 collected on February 22, 2005, from a collapsed part of spine 4—confirm the wide range in grain size of the gouge (fig. 17*A*). The two samples differ, however, in the extent of comminution. Sample SH307-1 has a bimodal size distribution with peaks at 10 and 350 μm ; it has very little material <1 μm in size and

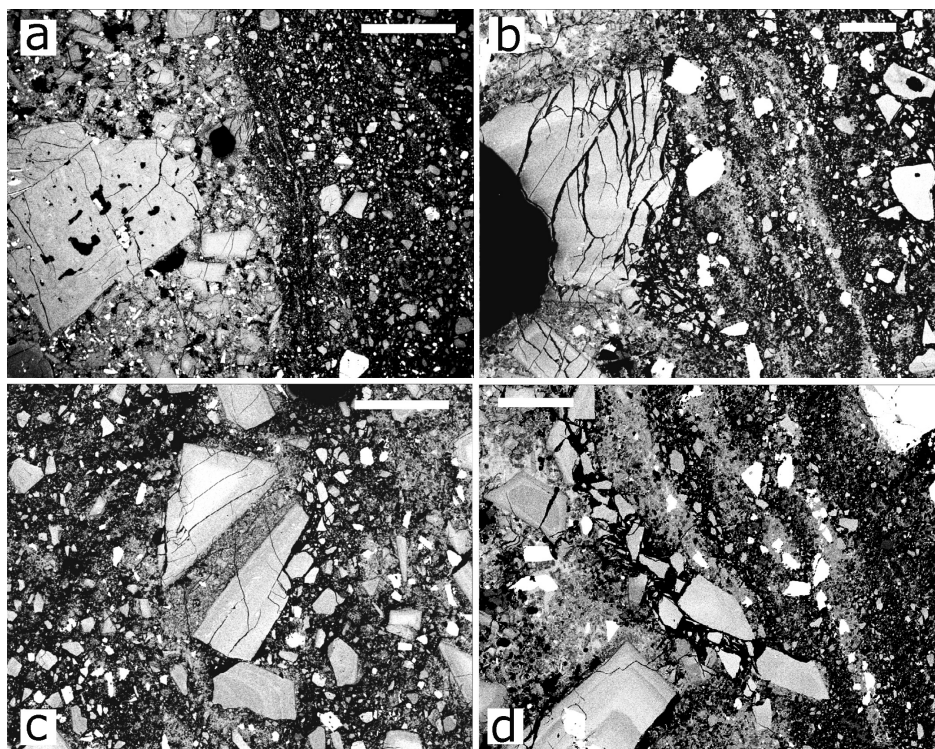


Figure 15. BSE images showing details of lava-cataclasite boundary preserved in sample SH324-4A, from spine 7 (see fig. 9b for smaller-scale view of boundary). *A*, Low-magnification image across boundary showing coherent dacite on left and cataclasite on right. Scale bar=1 mm. *B*, highly magnified view of boundary (from upper center of *A*) showing extensive fragmentation of a crystal next to boundary and thin slivers of intact holocrystalline matrix parallel to boundary. Scale bar 100 μm . *C*, lava fragment that shows (Reidel?) fractures through plagioclase microphenocrysts and holocrystalline matrix within gouge. Scale bar 250 μm . *D*, Broken slivers of holocrystalline matrix just below image of *B* that show lateral entrainment of broken crystal fragments into boundary zone. Scale bar 100 μm .

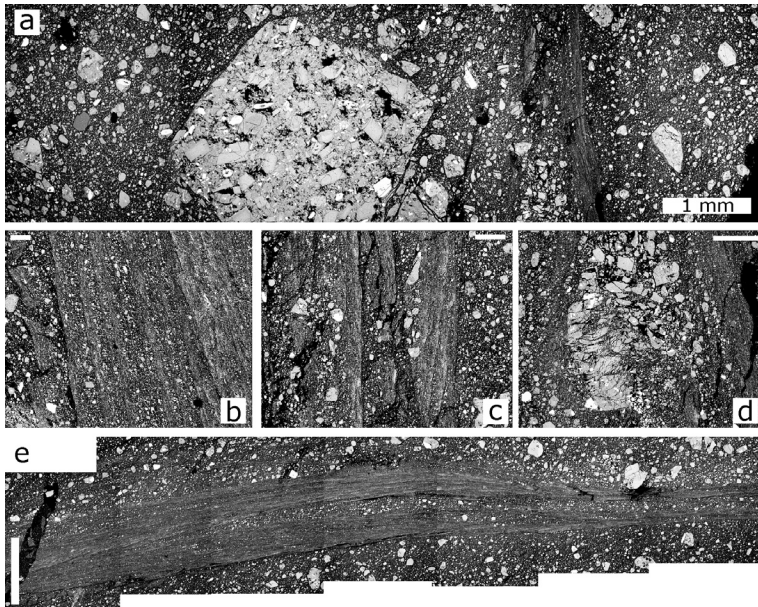


Figure 16. Backscattered electron images showing details of fault gouge sample SH313-1 from spine 4 (see fig. 9D for smaller-scale view). *A*, Transect across part of thin section SH313-1C showing wide range of clast sizes in gouge and extreme grain-size reduction within the ‘fault core,’ right of center. *B*, Detailed image of fine-scale foliated fault gouge showing slight offset in foliation orientation across image. Scale bar=100 μm . *C*, Breakage, disruption and partial rotation of finely pulverized gouge. Scale bar=200 μm . *D*, Shattered lava fragment adjacent to fault core. Scale bar=500 μm . *E*, Composite transect along fault zone in thin section SH313-1A. Note fine-scale foliation with orientation subparallel to fault zone and anastomosing strands that isolate regions of less extensively pulverized gouge fragments. Scale bar=1 mm.

measurable clasts $>5\text{mm}$. In contrast, the granulometric analysis for SH303-1 describes a rather broad peak with a poorly defined mode at about 32 μm , a substantial proportion of very fine grains, and no clasts $>2.8\text{ mm}$. This difference is best illustrated in a plot of cumulative volume, which shows the pronounced difference in volumetric contribution of very small particles (fig. 17B).

Grain size of fragments can also be estimated by analysis of BSE images. Although measurements of the number of clasts of a given size in area fraction is not directly comparable to measurement of the weight percent of a given sieve size, the image-analysis data provide another view of grain size characteristics that can be directly compared with data from tectonic faults. Illustrative measurements on images from SH326-2a (figs. 3, 8A, 9C) show that the number-based data are dominated by the smallest size classes, which are difficult to measure accurately. When viewed as areal abundance, the data show a mode at 500 μm , similar to the volume-based (sieve) data for SH307-1 (fig. 18A). These data lack an equivalent peak at 8 μm because this was below our detection limit ($\sim 30\text{ }\mu\text{m}$) for the imaging magnification used.

Quantifying the transition from intact dome lava to powdery gouge is more difficult. We experimented with measuring the reduction in size and abundance of plagioclase phenocrysts in thin section, a measurement that is easy to make using standard image analysis techniques. The overall abundance of plagioclase, as measured in full thin section scans (for example, fig. 9), decreases from a maximum of 32 percent in sample SH324-4a to 9.5 percent in consolidated gouge from the same sample (for example, fig. 9B; table 1). This range encompasses that of all other samples. Accompanying

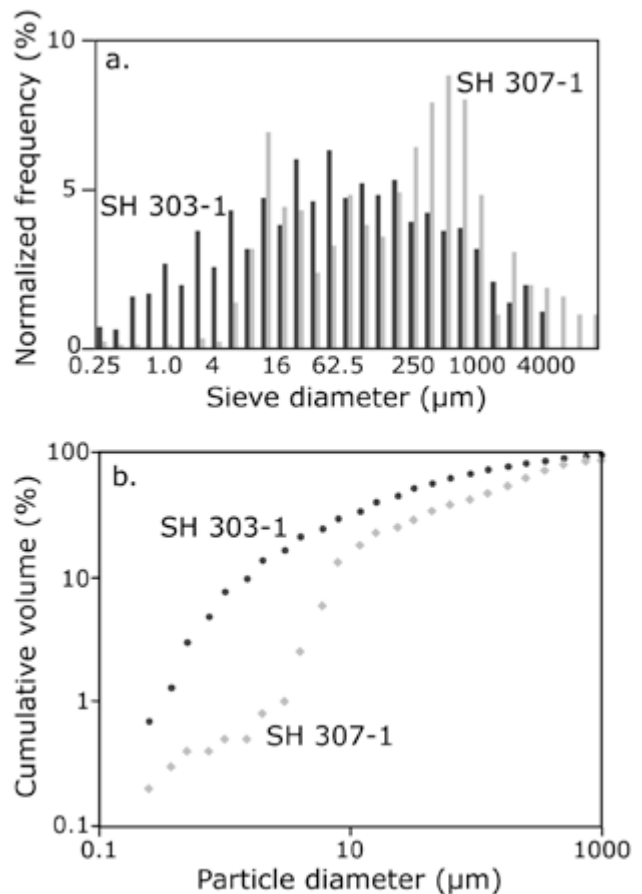


Figure 17. Sieve data for unconsolidated fault gouge samples SH303-1 (spine 3) and SH307-1 (spine 4). *A*, Histograms. *B*, Power-law plots. Note difference in abundance of very fine particles ($<10\text{ }\mu\text{m}$) in the two samples; also absence of single power-law trend.

the decrease in crystal abundance is a decrease in average phenocryst size, which reflects breakage of large crystals to form numerous small crystal fragments. This breakage most severely affects the large phenocrysts, as shown by normalized cumulative plagioclase volume distributions (fig. 19). From figure 19 it is clear that the median (50th percentile) plagioclase size decreases from about 300 μm in competent dome lava to about half of that in partially comminuted cataclasite sample 324-4a. More striking is the difference in maximum crystal size, which reaches several millimeters in the dome lava but only about 300 μm in SH324-4a cataclasite (table 1). If this analysis were extended to measurement of the finely laminated ultracataclasite zone of sample SH313-1 (fig. 16), the plagioclase size reduction would be even more extreme.

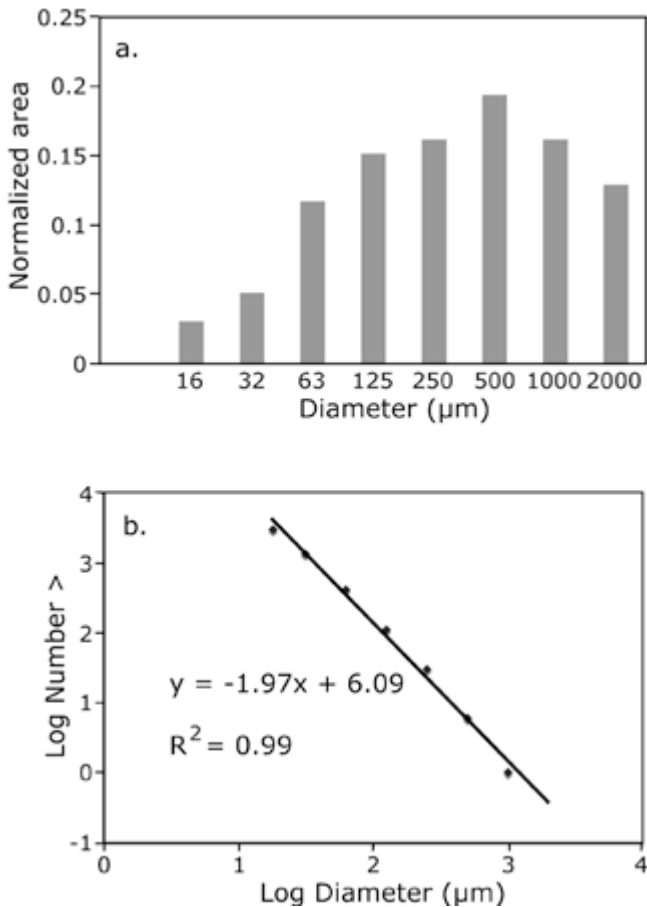


Figure 18. Grain size data obtained by image analysis of BSE image of SH 326-4A from spine 7. *A*, Histogram of data plotted by area (related to but not directly equivalent to volume-based sieve data). *B*, Power-law plot, with y-axis showing cumulative number of fragments greater than a given size. Data fit a power-law distribution over size range 10–1000 μm .

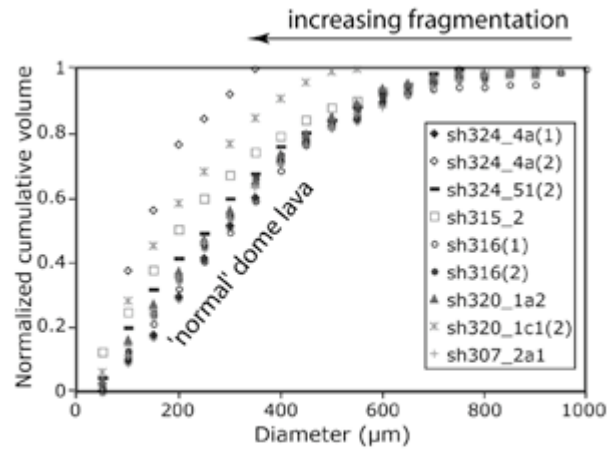


Figure 19. Plagioclase size distributions plotted as normalized cumulative volume for comparison with sieve data. Distributions determined by image analysis of full thin section images, as shown in figure 9. Minimum size resolution approximately 30 μm (microphenocrysts and phenocrysts). Data show that plagioclase size distributions of undeformed dacite lava change progressively with increasing fragmentation toward smaller median and maximum crystal diameters. This change in size distribution is accompanied by a decrease in overall abundance of macroscopic plagioclase.

In summary, we have experimented with different ways of quantifying the observed fragmentation of competent dome rocks. Grain size changes in fault gouge are typically measured by sieving, although this is possible only for unconsolidated samples. In cataclasite, clast size distributions may be measured in BSE images, although complete sample characterization using this method would require combination of multiple images at different magnifications. A simple characterization of progressive cataclasis of dome lava can be made using thin section measurements of plagioclase phenocryst size and abundance. Taken together, these various methods testify to extensive fragmentation and grain-size reduction of dome lava during transport to the surface.

Table 1. Plagioclase phenocryst and microphenocryst data obtained from image analysis of whole thin section scans.

[An example scan is shown in figure 9. Reported are the measured plagioclase area fraction, the total area measured (in mm²), the total number of crystals measured, the average crystal number per area (mm²), and the maximum and minimum crystal diameter (d) in mm. Where abrupt textural changes were preserved within a single thin section (for example, fig. 9B), different textural regimes were measured separately (denoted a and b).]

Sample No.	Plagioclase area fraction	Total area mm ²	Total number of crystals	Average crystal number	Maximum diameter	Minimum diameter
SH315	26.2	355	1692	4.77	3.32	0.1
SH316(1)	27.9	222.5	2441	10.97	1.19	0.03
SH316(2)	25.2	219.37	2389	10.89	0.85	0.03
SH320_1C1(1)	11.7	185.54	2404	12.96	1.01	0.02
SH320_1C1(2)	12.1	174.67	2253	12.90	0.624	0.02
SH320_1A2	21.5	250.75	3068	12.24	1.32	0.02
SH324_4a(1)	24	40.58	324	7.98	0.73	0.04
SH324_4a(2)	9.5	27.19	289	10.63	0.34	0.04
SH324_4b(1)	32	143.83	1772	12.32	1.43	0.04
SH324_4b(2)	19.3	87.41	1324	15.15	0.608	0.04
SH324_51(1)	25.8	198.9	3496	17.58	0.91	0.02
SH324_51(2)	24.2	125.37	1974	15.75	1.22	0.02
SH307_2A1	22.4	479.98	3330	6.94	2.27	0.05

Moreover, BSE images show that textural transitions are commonly abrupt, indicating extreme shear localization during transport. When combined with BSE evidence of initial grain shattering (figs. 15B, 16D) followed by shear, grinding, and wear (fig. 14B, C), these data suggest extensive transport distances (large strains) after initial breakage.

Discussion

The results presented above illustrate the range of processes that contributed to the transformation of dome lava to fault gouge and, in some cases, to ash emitted by small dome explosions (Rowe and others, this volume, chap. 29). Here we examine those processes in detail, paying particular attention to the role of degassing-induced crystallization and to conditions of fault formation. We then generalize these observations, placing them first within the perspective provided by past activity (1980–1986) at Mount St. Helens and then within the context of other spine-forming eruptions.

The role of decompression-crystallization

All clasts within both cataclasite and fault gouge are nearly holocrystalline. Thus we infer that fragmentation of dome dacite occurred after most of the groundmass had crystallized. Extensive crystallization is most likely caused by decompression and degassing during the slow ascent of hydrous magma (reviewed above), although we cannot rule out the possibility of minor late-stage cooling along the conduit margin. Extensive crystallization, in turn, changes the rheology of the rising magma, particularly when coupled with changes in melt viscosity resulting from volatile exsolution (for example, Hess and Dingwell, 1996; Melnik and Sparks, 2002, 2005). At Mount St. Helens, these rheological changes transformed the deformation properties of the magma from plastic to brittle, fragmenting the rising magma plug and creating the resultant thick fault gouge. Constraining the depth at which this transformation initiates is important for accurate modeling of dome extrusion (Iverson and others, in press), as well as for recognizing conditions that might lead to changes in the current eruptive activity.

Interpretation of the crystallization history of 2004–2006 Mount St. Helens dacite is complicated by

abundant evidence of nonequilibrium crystallization conditions, including (1) rapid late-stage growth of rims on plagioclase phenocryst (fig. 10); (2) spatial heterogeneity of groundmass textures (both vesicles and crystals; fig. 11); (3) the presence of two or, sporadically, three, silica phases (fig. 12); and (4) local temperature increases in the groundmass as the result of latent heat released by rapid groundmass crystallization (Blundy and others, this volume, chap. 33; Pallister and others, this volume, chap. 30). Here we briefly review the evidence for each before discussing the likely importance of each process to gouge formation.

Phenocryst textures that suggest rapid late-stage growth include swallowtail-like extensions from the corners of large crystals, irregular growth boundaries, and skeletal overgrowths that either partially or completely trap residual melt (fig. 10). These irregularities preserve glass within the growth protrusions, suggesting entrapment at moderately high pressures (that is, during early phases of groundmass crystallization), perhaps because microlite nucleation was inhibited by local increases in H₂O rejected from the rapidly growing crystal. Therefore it appears that this crystallization, while rapid, was not directly responsible for cataclasis and gouge formation, although it does reflect the overall importance of decompression-induced crystallization during this remarkably steady effusive activity.

More important for determining conditions of marginal fragmentation is the spatial inhomogeneity of groundmass textures found within the early dome lavas. Lavas are heterogeneous in both groundmass crystallinity and vesicularity. Heterogeneity in groundmass crystallinity is particularly evident in the concentration of cotectic quartz-plagioclase intergrowths along euhedral phenocryst margins (fig. 11). However, as most of the groundmass within the cataclasite and gouge samples is holocrystalline, it is unclear what effect, if any, the heterogeneities in groundmass crystallization may have had on brittle deformation of the dome dacite. Heterogeneous vesicle textures are more likely to affect the material properties of the lava when deformed. A feature of many of the holocrystalline clasts within the gouge is the presence of numerous tiny microvesicles that are probably a feature of second boiling during the last stages of crystallization. It is possible that variations in vesicle structure may play a role in clast breakage, although our observations suggest that this, also, does not dominate the failure behavior.

Most important for gouge formation seems to be near-complete solidification of the ascending magma. The depth of this solidification may be estimated

using both groundmass phases and crystal textures. Three silica phases occur within the matrix of different gouge clasts: cristobalite, tridymite, and quartz. Cristobalite typically forms large crystals; similar crystals in cryptodome dacite from the 1980 eruption were interpreted by Hoblitt and Harmon (1993) to result from vapor-phase crystallization. Quartz may also form discrete groundmass crystals but most commonly grows as fine-scale cotectic aggregates with plagioclase and anorthoclase. Tridymite forms discrete acicular grains (fig. 12) that are common in some samples, sparse in others, and completely absent in some dome lava. In their study of Mount St. Helens lava samples from 1980–1986, Blundy and Cashman (2001) found tridymite in a single lava sample erupted during the period of continuous slow effusion in 1983. They used experimental data to argue that equilibrium crystallization of tridymite in H₂O-saturated anorthite-free melts requires a minimum pressure of 11 MPa and temperature of 885°C. Addition of anorthite to the melt will increase the temperature of the high quartz-tridymite boundary. Subsequently Cashman and McConnell (2005) found additional examples of tridymite-bearing dacite from pyroclasts stored temporarily at shallow levels prior to explosive eruptions of Mount St. Helens during the summer of 1980. When analyzed for volatile content using FTIR, one such glassy sample preserved ~0.6 wt percent H₂O, suggesting a minimum pressure of 5 MPa (A. Rust, oral commun., 2005). Thus it appears that the presence of tridymite requires shallow (<25 MPa) but not surface (>5–10 MPa) pressures (depths between 200 and 1000 m for an average magma density of 2500 kg/m³). Patterns of silica-phase precipitation thus suggest (1) substantial delays in quartz nucleation to produce the observed high degree of spatial variability; (2) varying P-T paths during decompression, as illustrated by differences in the proportions of silica phases among samples; and (3) tridymite crystallization under a limited range of P-T conditions.

Experimental data (Hammer and Rutherford, 2002; Couch and others, 2003; Martel and Schmidt, 2003) further suggest that the common groundmass texture of holocrystalline quartz and feldspar intergrowths requires pressures >10 MPa (400 m) and crystallization time scales of weeks. If magma ascends at a constant rate from a storage region at >4 km (Rutherford and Devine, this volume), measured extrusion rates of ~7 m/d allow sufficient time for shallow crystallization (~3 months for ascent from 1000 to 400 m). Pressures as low as 5 MPa were also required to precipitate quartz-alkali feldspar intergrowths in decompression experiments on Pinatubo magma compositions (Hammer

and Rutherford, 2002), whereas maximum rates of plagioclase nucleation typically require pressures between 25 and 5 MPa (Hammer and Rutherford, 2002; Couch and others, 2003; Martel and Schmid, 2003). If gouge forms only after crystallization of the groundmass is nearly complete, these data suggest a shallow origin for the onset of brittle deformation (<400–500 m), consistent with the plug model of Iverson and others (in press). We note, however, that all of these estimates assume only minor cooling of magma during ascent, an assumption that appears reasonable given the high surface temperatures measured by FLIR (Schneider and others, this volume, chap. 17) and high Fe-Ti oxide temperatures from the dacite (Pallister and others, this volume, chap. 30).

Fault gouge formation

Extensive research on tectonic fault zones provides a framework for examining gouge formation during the extrusion of the 2004–2006 Mount St. Helens spines. Tectonic fault zones are commonly characterized by narrow (millimeter to centimeter) slip planes composed of finely pulverized rock surrounded by broader cataclasite zones (typically meters in scale and locally foliated) mantled outward by a zone of less intensely deformed rock (for example, Chester and Logan, 1986, 1987; Chester and others, 1993; Schulz and Evans, 1998; Storti and others, 2003). This fault-zone architecture is taken as evidence of strain-weakening behavior, with shear localization into narrow zones that act as the primary slip surfaces (for example, Ben-Zion and Sammis, 2003). Fault initiation in porous material commences with dispersed breakage, porosity reduction, and temporary strain hardening (for example, Mair and others, 2000; Cashman and Cashman, 2000). A change to strain-weakening behavior requires localization of shear through nucleation of interconnected slip surfaces (Biegel and others, 1989; Shipton and Cowie, 2003). Average particle size decreases with increasing strain (Marone and Scholz, 1989; Mair and others, 2000; Hadizadeh and Johnson, 2003) until that strain can be accommodated by rolling (Morgan and Boettcher, 1999), contact creep (Prasher, 1987), or development of new fault strands (if band formation results in local strain hardening; Mair and others, 2000).

In tectonic fault zones, gouge thickness shows a weak dependence on total displacement, a correlation that has been attributed to breakage of increasingly large asperities (Power and others, 1988). Sibson (1986) recognized three different types of natural fault gouge:

1. *Attrition breccia* resulting from wear. This gouge

type is rare in tectonic faults, characterized by rolled clasts, and associated only with zones of significant fault slip.

2. *Distributed crush breccia* formed by destruction of local asperities. This gouge type is characterized by pervasive microfractures and jigsaw textures.
3. *Implosion breccia*. Textures similar to those of distributed crush breccia.

Gouge within the cores of tectonic faults may contain ultrafine grains (micron to nanometer scale) whose origin has been variously attributed to quasi-static wear and attrition (Sammis and others, 1986; Chester and Chester, 1998), dynamic pulverization resulting from a single rupture event (Reches and Dewers, 2005; Wilson and others, 2005), and large strains (for example, Yund and others, 1990).

Our textural observations of cataclasite and gouge samples from Mount St. Helens provide an interesting perspective on fault gouge formation. Macroscopically, the structure of the fault zone along the conduit margin (for example, fig. 6) is similar to examples described in the fault literature, with an outer breccia that changes to cataclasite and finally into fault gouge containing slickensides, or areas of slip localization (figs. 8C, 16A) at the margin. Microscopically, localized extreme grain size reduction along slickensides is consistent with experimental generation of ultrafine grains by large shear strains (Yund and others, 1990). Using the correlation for tectonic faults, a gouge thickness of 1–3 m suggests displacements of <1000 m, in agreement with petrologic assessments of the depth of gouge formation presented above. Moreover, these values suggest total strains (displacement/thickness) less than or about 500. If we assume that all of the slip is concentrated along the conduit margin, observed slip rates of $\sim 8 \times 10^{-5}$ m/s are orders of magnitude higher than those of creeping faults and orders of magnitude lower than slip events on stick-slip faults. These slip velocities suggest strain rates (velocity/thickness) of $3\text{--}8 \times 10^{-5}$ /s, intermediate to values typical for creeping and stick-slip tectonic faults.

The fault gouge itself appears to represent at least two of Sibson's (1986) types. Extensive grain fragmentation adjacent to the slickenside zones (figs. 15B, 16D) fits Sibson's description of distributed crush breccia, in that individual pieces of a grain have not been displaced from each other by shear. However, it is clear that these fragments are eventually distributed along the foliation bands by shear displacement after crushing (figs. 15D, 16B, 16C). In contrast, the common rounded fragments in both cataclasite and gouge (figs. 14B, 14C) appear to be attrition breccia, with rounding the result of

abrasion and wear during shear transport. The prevalence of these attrition features may reflect not only the large total displacements (shear strain) involved with dome emplacement but also the steadiness of movement. Whereas sporadic movement of tectonic faults allows healing or lithification of fault zones between slip events, steady movement of solidified magma along the conduit margin apparently prevents such healing. Instead, the observed gradual decrease in the percentage of larger clasts apparently allows them to be isolated from each by the matrix, thus permitting individual clasts to roll and abrade. Continued brittle deformation of fragmented particles results in further grain size reduction and shear localization along multiple slickensides.

An interesting discussion in the fault zone literature involves the mechanism by which fragmentation occurs. Patterns of grain size reduction may be characterized by the fractal dimension D of particle grain size, where D relates cumulative particle frequency $N(S)$ (the number of particles less than S) to size (S):

$$N(S) \approx S^{-D}. \quad (1)$$

Thus D describes the relative proportion of small and large fragments; higher D values reflect samples where the grain size distribution is dominated by smaller particles. Within this framework, the ‘pillar of strength’ model (Allegre and others, 1982) predicts $D = 1.97$, the ‘plane of fragility’ model (Turcotte, 1986) predicts $D = 2.84$, and the constrained comminution model (Sammis

and others, 1986; Sammis and others, 1987; Sammis and Biegel, 1989; Turcotte, 1992) predicts $D = 2.6$. The latter model is based on sequential breakage of equal-size particles into a discrete (and relatively small) number of particles. Key to the constrained comminution model is that fragments of similar size are evenly distributed in space. Experimental studies of sheared quartz sand support a model of constrained comminution under conditions of high confining pressure (100 MPa) and particle size range of 10 μm to 1 mm (Biegel and others, 1989; Marone and Scholz, 1989). However, data from natural cataclastic samples are less easily interpreted (for example, Blenkinsop, 1991; An and Sammis, 1994; Storti and others, 2003; Cashman and others, in review). In many fault zones, D values change from low in brecciated damage zones to high in intensely comminuted narrow shear zones (fig. 20). These high D values (high degrees of crushing) may result from slip-enhanced surface abrasion during shear transport, as suggested by Hooke and Iverson (1995) for glacially abraded sediment. High degrees of crushing also create the matrix support required to allow rolling and abrasion of remaining larger particles.

The fragmentation schematic shown in figure 20 provides a description of the process of gouge development at Mount St. Helens. Imaging data, which can be used to characterize the larger clast sizes, yield fractal dimensions ~ 1.97 for particles from 10 to 1000 μm in diameter (fig. 18B). This low D value is consistent with the ‘pillar of strength’ model (Allegre and others, 1982) and similar to particle size distributions created by particulate flow of poorly lithified sediment at low confining pressures (<20–30 MPa; Rawling and Goodwin, 2003). Sieve data, however, show that grain size data are self similar (fractal) only over limited size ranges. As seen in other fault rocks, fits to straight-line segments suggest that D increases with decreasing grain size (for example, Blenkinsop, 1991; An and Sammis, 1994; Storti and others, 2003). High D values at very small grain sizes result from extensive comminution of individual clasts, as evidenced by the shattered large crystals and dome fragments that border the slickensides (figs. 15B, 16D). Thus we would interpret the grain size data to reflect (1) cataclasis and particulate flow (low D) over most of the observed gouge thickness and (2) strain localization and intense comminution within the slickensides, which are themselves distributed within the outer gouge zone.

The frictional properties of 2004–2005 Mount St. Helens fault gouge have been investigated by Moore and others (this volume, chap. 20) at room temperature, shear rates of $1.5\text{--}5000 \times 10^{-6}$ m/s and low normal stresses

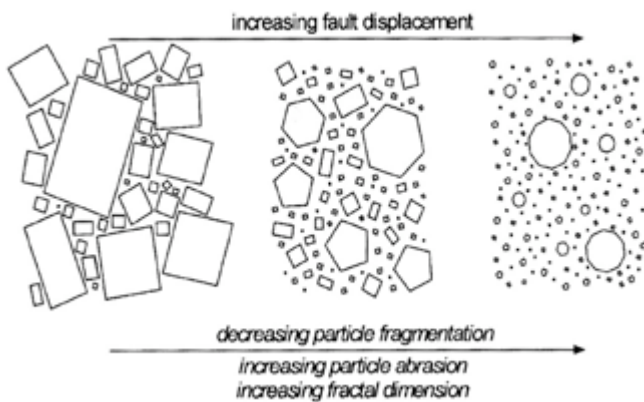


Figure 20. Cartoon showing schematic change in size and shape of grains with increasing fault displacement. Although drawn for tectonic faults, this progression from coarse to fine grain sizes and angular to rounded shapes appears appropriate to fault behavior associated with spine emplacement at Mount St. Helens. Figure from Storti and others (2003).

(5–195 kPa). They find rate-weakening behavior at shear rates $<1 \times 10^{-4}$ m/s and rate-strengthening behavior at $>5 \times 10^{-4}$ m/s, with stick-slip oscillations observed at the highest normal stress and lowest shear rates. However, although they observe shear localization into a narrow (1 mm) zone, they see no evidence of comminution or crushing of gouge, perhaps because the small cumulative strains and low normal stresses in the experiments were insufficient to produce the grain breakage observed in natural samples.

In summary, the unusually well developed fault gouge that has mantled all of the 2004–2006 Mount St. Helens spines provides evidence of profound change in the rheological behavior of dome lava during ascent as a consequence of near-complete crystallization and subsequent brittle breakage and gouge formation. The effect of this extensive brittle deformation on dome extrusion is less clear. Iverson and others (in press) suggest that rate-weakening behavior is required to produce the stick-slip behavior suggested by the repetitive (drumbeat) earthquakes. Alternatively, Mastin and others (this volume, chap. 22) call on a gouge zone that is, overall, rate strengthening but that fails in a patchwork fashion during extrusion. Field evidence for localized failure includes both observed Reidel shears in the cataclasite and throughgoing ultracataclasite (slickenside) bands within the gouge.

Comparison with other dome eruptions

The morphology and emplacement conditions of other recent domes and spines of intermediate composition are reviewed above. Here we use observations from the 2004–2006 activity at Mount St. Helens to evaluate processes that may have affected extrusive behavior at other volcanoes.

Dome emplacement during the 1980–1986 eruption of Mount St. Helens provides the most obvious comparison with current (2004–2006) activity. Importantly, although the erupted composition in the 1980s was quite similar to that of the 2004–2006 dacite and average effusion rates were comparable (or slightly lower), the 1980–1986 magma had a higher temperature (880–900°C in the early 1980s compared with 840–850°C in 2004–2006) and extrusion was dominantly episodic rather than continuous. Spines were produced on only two occasions: (1) accompanying endogenous growth during continuous effusion in 1983 and (2) following a protracted, 17-day episode of (mostly endogenous) dome lobe formation in May 1985.

Backscattered electron images of a sample from the February 1983 spine look remarkably similar to early samples of the 2004 spine (compare fig. 21A with fig. 11C). In both samples the distribution of groundmass crystals is heterogeneous, with clean glass most common between microlites and microphenocrysts and cotectic assemblages of quartz and feldspar lining the crystal margins. In contrast, a marginal sample of the May 1985 spine is holocrystalline (fig. 21B), with the characteristic cotectic crystallization fabric seen in the more slowly extruded 2005–2006 spine samples.

However, there are two differences between the spine sample from May 1985 and those of the current eruption. First, the extremely fine-scale ‘myrmekitic’ textures occupying interstices between microlites in the May 1985 sample (and not observed in the 2004–2006 spine samples) suggest that preeruptive crystallization

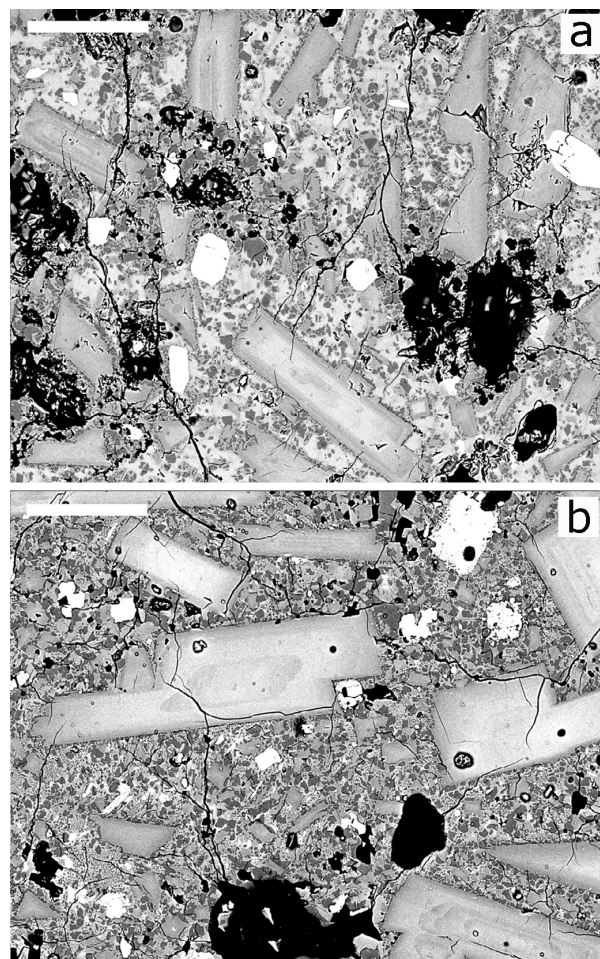


Figure 21. Backscattered electron images showing groundmass textures of 1980s lava spines of Mount St. Helens. Textures are similar to those observed in spines produced during current Mount St. Helens eruptive activity; for example, compare with figures 11C, 11D, 12A, or 12B. Scale bar=50 µm in each image. A, February 1983. B, May 1985.

occurred at very shallow levels, most likely within the dome itself. Second, the boundary between the extruded spine and the dome lobe had a very different character in 1985. In contrast to the thick gouge zones described above, the spine-dome lobe boundary in 1985 comprised a thin (~10 mm) cataclasite zone that, although showing some of the grain size reduction characteristics of the recent gouge, was much narrower and much less comminuted (compare thin section image of fig. 22 with those of fig. 9). These features suggest that the May 1985 dome was formed by very late stage solidification within the growing dome, with extrusion resulting in only small cumulative displacements (strain), consistent with its small size.

More similar are larger spines produced at Mont Pelée (1903), Unzen (1991–1995), and Soufrière Hills (1995–present), which have macroscopic features similar to the 2004–2006 spines at Mount St. Helens, including smooth curved forms and pronounced striations parallel to the extrusion direction (reviewed above). Descriptions in the literature suggest that gouge was present on the striated surface of the giant Mont Pelée spine (Jaggard, 1904); gouge and cataclasite also mantle some large dome fragments from Soufrière Hills, Montserrat. Conditions leading to spine formation also appear similar at all of these locations. Most important are estimated ascent rates of $1\text{--}3 \times 10^{-4}$ m/s, rates that are sufficiently slow for the extensive crystallization necessary for both plug and fault gouge formation (see above). The comparison between the 1985 and current spines at Mount St. Helens further suggests that formation of large spines requires that magma solidify well within the conduit. This depth of solidification, in turn, means that solid dome rock must be transported large distances before exiting the vent, with resulting large strains responsible for the development of thick

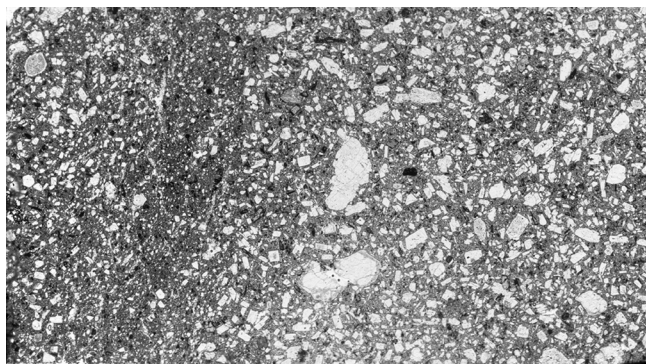


Figure 22. Full thin section scan of sample collected across margin of May 1985 dome lobe (right) and spine (far left). Darker area of reduced phenocryst size toward the left side of figure is thin (<1 cm) cataclasite zone that marks lava-spine boundary.

gouge zones.

From dome to dust

Is brittle deformation unique to holocrystalline spines of intermediate composition? The answer is clearly no, as numerous small-scale brittle deformation features have been described along shallow conduit margins and within basal shear zones of glassy obsidian domes, including anastomosing tuffisite veins and fractures, cataclasite zones, and trails of broken phenocrysts (for example, Stasiuk and others, 1996; Tuffen and Dingwell, 2005). Fracture and grain size reduction in these systems have been explained by shear-strain rates at conduit margins exceeding experimentally determined critical rates for shear-induced fragmentation (for example, Dingwell and Webb, 1989) of high viscosity ($10^{10}\text{--}10^{12}$ Pa s) melts at the low strain rates ($10^{-3}\text{--}10^{-5}$ /s) anticipated for dome extrusion (Gonnermann and Manga, 2003; Tuffen and others, 2003).

Deformation textures in obsidian domes, however, differ dramatically from those described here for the Mount St. Helens gouge zone. First, fracture networks in obsidian are limited to thin (< 20 mm) fault and injection veins with limited to no displacement and thicker, irregular “injection voids” (≤ 80 mm in width; Tuffen and Dingwell, 2005). The largest fault complex observed by Tuffen and Dingwell (2005) is ~5m in length, with a maximum offset of 0.13 m. Thus these features are substantially smaller than the zones of breccia, cataclasite, and gouge that line the shallow Mount St. Helens conduit, with the possible exception of basal breccia zones in some obsidian flows (Gonnermann and Manga, 2003). Moreover, both tuffisite veins and basal breccias show abundant evidence of annealing and ductile deformation (Gonnermann and Manga, 2003; Tuffen and others, 2003; Tuffen and Dingwell, 2005). In contrast, gouge zones at Mount St. Helens are dominated by brittle fracture and cataclastic flow, with no evidence of re-annealing between fracture events. Finally, fracture zones within obsidian domes appear to lack the distinct zones of breccia, cataclasite, and gouge seen at Mount St. Helens; instead fragment sizes within the tuffisite veins are very small (much less than 1 mm), with no clasts of intermediate size.

What are the implications of these differences in fragmentation style? First, the common annealing textures preserved within tuffisite veins and basal breccias related to obsidian flows result from the strain-dependent rheology of viscous silicate melts: at the same

temperature, the melt will flow at low strain rates but fracture at higher strain rates. For this reason, a model of flow emplacement by repeated fracture and healing *of the same magma* has been suggested for obsidian (Tuffen and others, 2003; Tuffen and Dingwell, 2005). This model has been extended to explain repetitive seismic events accompanying andesitic dome growth at Soufrière Hills, Montserrat (for example, Neuberg and others, 2006). Our observations of fault gouge formation would suggest caution, however, in direct application of deformation mechanisms in obsidian to the interpretation of seismicity associated with the emplacement of highly crystalline lava. Most importantly, we see no evidence of annealing within the gouge zone between fracture events. Instead, fault gouge forms by fracture and fragmentation of crystals and holocrystalline matrix into successively smaller fragments. For this reason, we suggest that the origin of the repetitive (drumbeat) earthquakes at Mount St. Helens most likely lies in progressive fragmentation of dome dacite rather than by process of repeated fracture and healing. Although definite assignment of individual slip features to specific earthquake characteristics is beyond the scope of this paper, we note that several types of slip zones are apparent at the outcrop to hand specimen scale, from Reidel shears in the cataclasite (fig. 6) to slickensides in the gouge (fig. 8C). If individual drumbeat earthquakes represent slip events of ~5 mm (Iverson and others, in press), then they may represent the composite effect of fracturing multiple smaller grains (as suggested by the dominance of fine (<10–20 µm) material within the cataclasite and gouge zone. Alternatively, perhaps only the initial fragmentation of larger dome fragments is seismogenic.

This leads to a final point—the role of fragmentation during dome explosions. A common assumption is that dome explosions result from sudden decompression of pressurized dome interiors and resultant brittle fragmentation (for example, Alidibirov and Dingwell, 1996). However, Rowe and others (this volume, chap. 29) demonstrate that ash released during the two substantial dome explosions associated with the current eruption (in January and March of 2005) bears a striking textural resemblance to the fault gouge described here. The implications of this observation are that the explosions themselves transported, but did not generate, much of the ash emitted during each event, an interpretation consistent with the source of the explosions at the junction of the spine and the conduit rather than from within the dome itself. In fact, we suspect that gouge formed along conduit margins may commonly supply ash to explosions that accompany spine growth (for example, Jaggar, 1904), a hypothesis

that suggests that further studies of the physical properties of volcanic gouge (especially relations between deformation behavior and permeability) could improve our understanding of hazards related to the slow extrusion of lava spines.

Conclusions

Here we have documented field, hand sample, and thin section evidence for cataclasis and gouge formation along the margins of the smooth-surfaced spines extruded from Mount St. Helens from 2004 to present. These observations show brittle breakage and subsequent cataclastic flow to be important in the slow extrusion of intermediate composition hydrous magma. Detailed textural observations document both crystallization accompanying magma ascent (decompression) and the sequential fragmentation of competent dome rock to produce fine-grained fault gouge. Taken together, these observations provide new constraints on interactions between rates of magma ascent, degassing, crystallization, and brittle fragmentation, interactions that control the dynamics of lava extrusion.

The groundmass of dacite lava samples is variably crystalline, with the extent of groundmass crystallinity apparently increasing with time (decreasing mass eruption rate). Most, if not all, of the crystallization is driven by decompression and degassing rather than cooling. In fact, if anything, Fe–Ti oxide temperatures suggest that the extensive crystallization may help to heat the magma (for example, Blundy and others, 2006; Pallister and others, this volume, chap. 30). Within the gouge zone, dome fragments are holocrystalline, indicating solidification along conduit margins prior to brittle fragmentation. Detailed textural observations show that the transformation of competent dacite to fine powder occurred by sequential breakage of rock fragments to form zones of breccia, cataclasite, and gouge. Further concentration of slip along narrow slickenside planes produced thin (1 mm) zones of pulverized and foliated ultracataclasite. Both the extreme grain size reduction along these slip zones and the shattering of individual grains observed adjacent to narrow slip surfaces are similar to textures observed in near-surface gouge produced by large tectonic faults (for example, Cashman and others, in review) and suggest large strains. This inference is reasonable given a solidification depth of 400–500 m, above which deformation is apparently concentrated along the conduit margin (for example, Iverson and others, in press). However, we see no evidence of subsequent

annealing, as is commonly observed in tuffisite veins and obsidian flows (for example, Tuffen and others, 2003; Gonnermann and Manga, 2003), suggesting that earthquake-generating mechanisms based on repeated fracturing and healing do not apply to the extrusion of highly crystalline domes. The two explosions that have occurred (in January and March of 2005) were located at the contact between the spine and conduit wall and ejected ash that appears to have originated as fault gouge.

The physical characteristics of dome extrusion at Mount St. Helens from 2004–2006 can be generalized to other recent examples of andesite and dacite extrusions. As surmised by Williams (1932), the complete decompression-driven solidification prior to magma extrusion necessary for spine formation requires magma ascent to be slow relative to the kinetics of crystallization and the dynamics of gas loss. Spine formation appears limited to magma ascent rates of $<1\text{--}5 \times 10^{-4}$ m/s, which allows several weeks for magma to transit from ~1000 m (the point at which crystallinity increases dramatically as a function of decreasing pressure; Blundy and others, 2006) to ~400 m, where extensive cotectic crystallization of quartz and feldspar occurs. Comparison of marginal shear behavior of a small spine produced at Mount St. Helens in 1985 and the large spines of 2004–2006 suggest a further point—that formation of large spines requires that solidification occur deep within the conduit, a condition that leads to extensive brittle deformation and gouge formation during transit to the surface.

Acknowledgments

The authors would like to acknowledge all CVO personnel who helped with field observations and sample collection, as well as a host of volunteers who helped to sort and catalogue the samples. Reviewers Rob Watts and Nick Beeler are thanked for their thoughtful comments on the first draft of the manuscript. K. Cashman acknowledges support from NSF EAR-0207362 and EAR-0510437.

References Cited

- Alidibirov, M., and Dingwell, D.B., 1996, Magma fragmentation by rapid decompression: *Nature*, v. 380, p. 146–148.
- Allegre, C.J., LeMouel, J.L., and Provost, A., 1982, Scaling rules in rock fracture and possible implications for earthquake predictions: *Nature*, v. 297, p. 47–49.
- An, L.J., and Sammis, C., 1994, Particle size distribution in cataclastic fault materials from Southern California: a 3-D study: *Pure and Applied Geophysics*, v. 143, p. 203–228.
- Ben-Zion, Y., and Sammis, C., 2003, Characterization of fault zones: *Pure and Applied Geophysics*, v. 160, p. 677–715.
- Biegel, R., Sammis, C., and Dieterich, J.H., 1989, The frictional properties of a simulated fault gouge having a fractal particle distribution: *Journal of Structural Geology*, v. 11, p. 827–846.
- Blenkinsop, T.G., 1991, Cataclasis and processes of particle size reduction: *Pure and Applied Geophysics*, v. 136, p. 59–86.
- Blundy, J., and Cashman, K.V., 2001, Ascent-driven crystallisation of dacite magmas at Mount St. Helens, 1980–1986: *Contributions to Mineralogy and Petrology*, v. 140, p. 631–651.
- Blundy, J., and Cashman, K.V., 2005, Rapid decompression crystallization recorded by melt inclusions from Mount St. Helens volcano: *Geology*, v. 33, p. 793–796.
- Blundy, J., Cashman, K., and Humphreys, M., 2006, Magma heating by decompression-driven crystallization beneath andesite volcanoes: *Nature*, v. 443, p. 76–80, doi:10.1038/nature05100.
- Blundy, J., Cashman, K.V., and Berlo, K., 2007, Evolving magma storage conditions beneath Mount St. Helens inferred from chemical variations in melt inclusions from the 1980–1986 and current eruptions, chap. 33 in Sherrod, D.R., Scott, W.E., and Stauffer, P.H., eds., *A volcano rekindled: the first year of renewed eruption at Mount St. Helens, 2004–2006*: U.S. Geological Survey Professional Paper (this volume).
- Cashman, K.V., 1992, Groundmass crystallization of Mount St. Helens dacite, 1980–1986: A tool for interpreting shallow magmatic processes: *Contributions to Mineralogy and Petrology*, v. 109, p. 431–449.
- Cashman, K.V., and Blundy, J., 2000, Degassing and crystallization of ascending andesite and dacite: *Philosophical Transactions of the Royal Society of London*, v. 358, p. 1487–1513.
- Cashman, K.V., and McConnell, S., 2005, Multiple levels of magma storage during the 1980 summer eruptions of Mount St. Helens, WA: *Bulletin of Volcanology*, v. 68, p. 57–75.
- Cashman, S.M., and Cashman, K.V., 2000, Cataclasis and deformation-band formation in unconsolidated marine terrace sand, Humboldt County, California: *Geology*, v. 28, p. 111–114.
- Cashman, S.M., Baldwin, J.N., Cashman, K.V., Swanson, K.R., Crawford, R., and Deis, A., Microstructures developed by coseismic and aseismic faulting in unconsolidated near-surface sediments, San Andreas fault, California: (in review, *Geology*).
- Chadwick, W.W., Archuleta, R.J., and Swanson, D.A., 1988, The mechanics of ground deformation precursory to dome-building extrusions at Mount St. Helens 1981–1982: *Journal of Geophysical Research*, v. 93, p. 4351–4366.

- Chester, F.M., and Logan, J.M., 1986, Implications for mechanical properties of brittle faults from observations of the Punchbowl fault zone, California: *Pure and Applied Geophysics*, v. 124, p. 79–106.
- Chester, F.M., and Logan, J.M., 1987, Composite planar fabric of gouge from the Punchbowl fault, California: *Journal of Structural Geology*, v. 9, p. 621–634.
- Chester, F.M., Evans, J.P., and Beigel, R.L., 1993, Internal structure and weakening mechanics of the San Andreas Fault: *Journal of Geophysical Research*, v. 98, p. 771–786.
- Couch, S., Sparks, R.S.J., and Carroll, M.R., 2003, The kinetics of degassing-induced crystallization at Soufrière Hills Volcano, Montserrat: *Journal of Petrology*, v. 44, p. 1477–1502.
- Devine, J.D., Rutherford, M.J., Norton, G.E., and Young, S.R., 2003, Magma storage region processes inferred from geochemistry of Fe–Ti oxides in andesitic magma, Soufrière Hills volcano, Montserrat, W.I.: *Journal of Petrology*, v. 44, p. 1375–1400.
- Dingwell, D.B., and Webb, S.L., 1989, Structural relaxation in silicate melts and non-Newtonian melt rheology in geological processes: *Physics and Chemistry of Minerals*, v. 16, p. 508–516.
- Donnadieu, D., and Merle, O., 1998, Experiments on the indentation process during cryptodome intrusions: New insights into Mount St. Helens deformation: *Geology*, v. 26, p. 79–82.
- Endo, E.T., Dzurisin, D., and Swanson, D.A., 1990, Geophysical and observational constraints for ascent rates of dacitic magma at Mount St. Helens, *in* Ryan, M.P., ed., *Magma Transport and Storage*: New York, John Wiley, p. 318–334.
- Fink, J.H., Malin, M.C., and Anderson, S.W., 1990, Intrusive and extrusive growth of the Mount St Helens lava dome: *Nature* v. 348, p. 435–437.
- Gardner, C.A., Cashman, K.V., and Neal, C.A., 1998, Tephra-fall deposits from the 1992 eruption of Crater Peak, Alaska: implications of clast textures for eruptive processes: *Bulletin of Volcanology*, v. 59, p. 537–555.
- Geschwind, C.-H., and Rutherford, M.J., 1995, Crystallization of microlites during magma ascent: the fluid mechanics of 1980–1986 eruptions at Mount St. Helens: *Bulletin of Volcanology*, v. 57, p. 356–370.
- Gilbert, G.K., 1904, The mechanism of the Mont Pelée spine: *Science*, v. 19, p. 927–928.
- Gonnermann, H.M., and Manga, M., 2003, Explosive volcanism may not be an inevitable consequence of magma fragmentation: *Nature*, v. 426, p. 432–435.
- Hadizadeh, J., and Johnson, W.K., 2003, Estimating local strain due to comminution in experimental cataclastic textures: *Journal of Structural Geology*, v. 25, p. 1973–1979.
- Hammer, J.E., and Rutherford, M.J., 2002, An experimental study of the kinetics of decompression-induced crystallization in silicic melt: *Journal of Geophysical Research*, v. 107, no. B1, doi:10.1029/2001JB000281, 24 p.
- Hammer, J.E., Cashman, K.V., and Voight, B., 2000, Magmatic processes revealed by textural and compositional trends in Merapi dome lavas: *Journal of Volcanology and Geothermal Research*, v. 100, p. 165–192.
- Hammer, J.E., Cashman, K.V., Hoblitt, R., and Newman, S., 1999, Degassing and microlite crystallization during the pre-climactic events of the 1991 eruption of the Mt. Pinatubo, Philippines: *Bulletin of Volcanology*, v. 60, p. 355–380.
- Heliker, C., 1995, Inclusions in Mount St. Helens dacite erupted from 1980 through 1983: *Journal of Volcanology and Geothermal Research*, v. 66, p. 115–135.
- Hess, K.-U., and Dingwell, D.B., 1996, Viscosities of hydrous leucogranitic melts: a non-Arrhenian model: *American Mineralogist*, v. 81, p. 1297–1300.
- Hoblitt, R.P., and Harmon, R.S., 1993, Bimodal density distributions of cryptodome dacite from the 1980 eruption of Mount St. Helens, Washington: *Bulletin of Volcanology*, v. 55, p. 421–437.
- Hooke, R.L., and Iverson, N.R., 1995, Grain-size distribution in deforming subglacial tills: role of grain fracture: *Geology*, v. 23, p. 57–60.
- Iverson, R.M., 2007, Dynamics of seismogenic volcanic extrusion resisted by a solid surface plug, Mount St. Helens, 2004–2005, chap. 21 *of* Sherrod, D.R., Scott, W.E., and Stauffer, P.H., eds., *A volcano rekindled: the first year of renewed eruption at Mount St. Helens, 2004–2005*: U.S. Geological Survey Professional Paper (this volume).
- Iverson, R.M., Dzurisin, Daniel, Gardner, C.A., Gerlach, T.M., LaHusen, R.G., Lisowski, Michael, Major, J.J., Malone, S.D., Messerich, J.A., Moran, S.C., Pallister, J.S., Qamar, A.I., Schilling, S.P., and Vallance, J.W., in press, Dynamics of seismogenic volcanic extrusion at Mount St. Helens in 2004–05: *Nature*.
- Jaggard, T.A., 1904, The initial stages of the spine on Pelée: *American Journal of Science*, v. 17, p. 34–40.
- Lacroix, A., 1904, *La Montagne Pelée et ses éruptions*: Paris, Masson et Cie, 62 p.
- Mair, K., Main, I., and Elphick, S., 2000, Sequential growth of deformation bands in the laboratory: *Journal of Structural Geology*, v. 22, p. 25–42.
- Marone, C.J., and Scholz, C.H., 1989, Particle-size distribution and microstructures within simulated fault gouge: *Journal of Structural Geology*, v. 11, p. 799–814.
- Martel, C., and Schmidt, B.C., 2003, Decompression experiments as an insight into ascent rates of silicic magmas: *Contributions to Mineralogy and Petrology*, v. 144, p. 397–415.
- Martel, C., Bourdier, J.-L., Pichavant, M., and Traineau, H., 2000, Textures, water content and degassing of silicic andesites from recent plinian and dome-forming eruptions at Mont Pelée volcano (Martinique, Lesser Antilles arc): *Journal of Volcanology and Geothermal Research*, v. 96, p.

- 191–206.
- Mastin, L.G., Roeloffs, E., Beeler, N.M., and Quick, J.E., 2007, Constraints on the size, overpressure, and volatile content of the Mount St. Helens magma system from geodetic and dome-growth measurements during the 2004–2006 eruption, chap. 22 *in* Sherrod, D.R., Scott, W.E., and Stauffer, P.H., eds., *A volcano rekindled: the first year of renewed eruption at Mount St. Helens, 2004–2006*: U.S. Geological Survey Professional Paper (this volume).
- Melnik, O., and Sparks, R.S.J., 2002, Dynamics of magma ascent and lava extrusion at Soufrière Hills Volcano, Montserrat: *Geological Society of London Memoir* 21, p. 153–171.
- Melnik, O., and Sparks, R.S.J., 2005, Controls on conduit magma flow dynamics during lava dome building eruptions: *Journal of Geophysical Research*, v. 110, p. 1–21.
- Metrich, N., Bertagnini, A., Landi, P., and Rosi, M., 2001, Crystallization driven by decompression and water loss at Stromboli Volcano (Aeolian Islands, Italy): *Journal of Petrology*, v. 42, p. 1471–1490.
- Moore, P.L., Iverson, N.R., and Iverson, R.M., 2007, Frictional properties of the 2004–2005 Mount St. Helens gouge, chap. 20 *in* Sherrod, D.R., Scott, W.E., and Stauffer, P.H., eds., *A volcano rekindled: the first year of renewed eruption at Mount St. Helens, 2004–2006*: U.S. Geological Survey Professional Paper (this volume).
- Moran, S.C., Malone, S., Qamar, A.J., Thelen, W., Wright, A.K., and Caplan-Auerbach, J., 2007, 2004–2005 Seismicity associated with the renewed dome-building eruption of Mount St. Helens, chap. 2 *in* Sherrod, D.R., Scott, W.E., and Stauffer, P.H., eds., *A volcano rekindled: the first year of renewed eruption at Mount St. Helens, 2004–2006*: U.S. Geological Survey Professional Paper (this volume).
- Morgan, J.K., and Boettcher, M.S., 1999, Numerical simulations of granular shear zones using the distinct element method. 1. Shear zone kinematics and the micromechanics of localization: *Journal of Geophysical Research*, v. 104, p. 2703–2719.
- Nakada, S., and Fujii, T., 1993, Preliminary report on the activity at Unzen Volcano (Japan), November 1990–November 1991: Dacite lava domes and pyroclastic flows: *Journal of Volcanology and Geothermal Research*, v. 54, p. 319–333.
- Nakada, S., and Motomura, Y., 1999, Petrology of the 1991–1995 eruption at Unzen: effusion pulsation and groundmass crystallization: *Journal of Volcanology and Geothermal Research*, v. 89, p. 173–196.
- Nakada, S., Miyake, Y., Sato, H., Oshima, O., and Fujinawa, A., 1999, Endogenous growth of dacite dome at Unzen volcano (Japan), 1993–1994: *Geology*, v. 23, p. 157–160.
- Nakada, S., Motomura, Y., and Shimizu, H., 1995, Manner of magma ascent at Unzen Volcano (Japan): *Geophysical Research Letters*, v. 22, p. 567–570.
- Neuberg, J.W., Tuffen, H., Collier, L., Green, D., Powell, T., and Dingwell, D., 2006, The trigger mechanism of low-frequency earthquakes on Montserrat: *Journal of Volcanology and Geothermal Research*, v. 153, p. 37–50.
- Newhall, C.G., and Melson, W.G., 1983, Explosive activity associated with the growth of volcanic domes: *Journal of Volcanology and Geothermal Research*, v. 17, p. 111–131.
- Pabst, A., 1931, Pressure-shadows and the measurement of the orientation of minerals in rocks: *American Mineralogist*, v. 16, p. 55–70.
- Pallister, J.S., Reagan, M., and Cashman, K., 2005, A new eruptive cycle at Mount St. Helens?: *Eos*, (American Geophysical Union Transactions), v. 86, no. 48, p. 499–500.
- Pallister, J.S., Thornber, C.R., Cashman, K.V., Clynne, M.A., Lowers, H.A., Brownfield, I.K., and Meeker, G.P., 2007, Petrology of the 2004–2006 Mount St. Helens lava dome-implications for magmatic plumbing, explosivity and eruption triggering, chap. 30 *in* Sherrod, D.R., Scott, W.E., and Stauffer, P.H., eds., *A volcano rekindled: the first year of renewed eruption at Mount St. Helens, 2004–2006*: U.S. Geological Survey Professional Paper (this volume).
- Power, W.L., Tullis, T.E., and Weeks, J.D., 1988, Roughness and wear during brittle faulting: *Journal of Geophysical Research*, v. 93, p. 15268–15278.
- Prasher, C.L., 1987, *Crushing and grinding process handbook*: New York, John Wiley, 482 p.
- Rawling, G.C., and Goodwin, L.B., 2003, Cataclasis and particulate flow in faulted, poorly lithified sediments: *Journal of Structural Geology*, v. 25, p. 317–331.
- Reches, Z., and Dewers, T.A., 2005, Gouge formation by dynamic pulverization during earthquake rupture: *Earth and Planetary Science Letters*, v. 235, p. 361–374.
- Rowe, M.C., Thornber, C.R., and Kent, A.J.R., 2007, Geochemistry of 2004–2005 Mount St. Helens ash: identification and evolution of the juvenile component, chap. 29 *in* Sherrod, D.R., Scott, W.E., and Stauffer, P.H., eds., *A volcano rekindled: the first year of renewed eruption at Mount St. Helens, 2004–2006*: U.S. Geological Survey Professional Paper (this volume).
- Rutherford, M.J., and Devine, J.D., 2007, Magmatic conditions and processes in the storage zone of the 2004–06 Mount St. Helens eruptions: the record in hornblende and plagioclase phenocrysts, chap. 31 *in* Sherrod, D.R., Scott, W.E., and Stauffer, P.H., eds., *A volcano rekindled: the first year of renewed eruption at Mount St. Helens, 2004–2006*: U.S. Geological Survey Professional Paper (this volume).
- Sammis, C., and Biegel, R., 1989, Fractals, fault gouge and friction: *Pure and Applied Geophysics*, v. 131, p. 255–271.
- Sammis, C., King, G., and Biegel, R., 1987, The kinematics of gouge deformation: *Pure and Applied Geophysics*, v. 125, p. 777–812.
- Sammis, C., Osborne, R.H., Anderson, J.L., Banerdt, M., and White, P., 1986, Self-similar cataclasis in the formation of fault gouge: *Pure and Applied Geophysics*, v. 143, p. 54–77.

- Schilling, S.P., Thompson, R.A., Messerich, J.A., and Iwatsubo, E.Y., 2007, Mount St. Helens lava dome growth and surface modeling, chap. 8 *in* Sherrod, D.R., Scott, W.E., and Stauffer, P.H., eds., *A volcano rekindled: the first year of renewed eruption at Mount St. Helens, 2004–2006*: U.S. Geological Survey Professional Paper (this volume).
- Schneider and others, 2007, [FLIR chapter], chap. 17 *in* Sherrod, D.R., Scott, W.E., and Stauffer, P.H., eds., *A volcano rekindled: the first year of renewed eruption at Mount St. Helens, 2004–2006*: U.S. Geological Survey Professional Paper (this volume).
- Scholz, C.H., 1990, *The mechanics of earthquakes and faulting*: New York, Cambridge University Press, 439 p.
- Schulz, S.E., and Evans, J.P., 1998, Spatial variability in microscopic deformation and composition of the Punchbowl fault, southern California: Implications for mechanism, fluid-rock interaction, and fault morphology: *Tectonophysics*, v. 295, p. 225–246.
- Scott and others, 2007 [Overview chapter], chap. 1 *in* Sherrod, D.R., Scott, W.E., and Stauffer, P.H., eds., *A volcano rekindled: the first year of renewed eruption at Mount St. Helens, 2004–2006*: U.S. Geological Survey Professional Paper (this volume).
- Shepherd, E.S., and Merwin, H.E., 1927, Gases of the Mt. Pelée lavas of 1902: *Journal of Geology*, v. 35, p. 97–116.
- Shipton, Z.K., and Cowie, P.A., 2003, A conceptual model for the origin of fault damage zone structures in high-porosity sandstone: *Journal of Structural Geology*, v. 25, p. 333–344.
- Sibson, R.H., 1977, Fault rock and fault mechanisms: *Journal of the Geological Society, London*, v. 133, p. 191–213.
- Sibson, R.H., 1986, Brecciation processes in fault zones: Inferences from earthquake rupturing: *Pure and Applied Geophysics*, v. 124, p. 159–176.
- Snoke, A.W., Tullis, J., and Todd, V.R., 1998, *Fault-related rocks: a photographic atlas*: Princeton, Princeton University Press, 617 p.
- Sparks, R.S.J., Murphy, M.D., Lejeune, A.M., Watts, R.B., Barclay, J., and Young, S.R., 2000, Control on the emplacement of the andesite lava dome of the Soufrière Hills volcano, Montserrat by degassing-induced crystallization: *Terra Nova*, v. 12, p. 14–20.
- Stasiuk, M.V., Barclay, J., Carroll, M.R., Jaupart, C., Ratte, J.C., Sparks, R.S.J., and Tait, S.R., 1996, Degassing during magma ascent in the Mule Creek vent (USA): *Bulletin of Volcanology*, v. 58, p. 117–130.
- Storti, F., Billi, A., and Salvini, F., 2003, Particle size distribution in natural carbonate fault rocks: insights for non-self-similar cataclasis: *Earth and Planetary Science Letters*, v. 206, p. 173–186.
- Streck, M.J., Broderick, Cindy, Thornber, C.R., Clynne, M.A., and Pallister, J.S., 2007, Plagioclase populations and zoning in dacites of the 2004–2005 Mount St. Helens eruption: constraints for magma origin and dynamics, chap. 34 *in* Sherrod, D.R., Scott, W.E., and Stauffer, P.H., eds., *A volcano rekindled: the first year of renewed eruption at Mount St. Helens, 2004–2006*: U.S. Geological Survey Professional Paper (this volume).
- Swanson, D.A., and Holcomb, R.T., 1990, Regularities in the growth of the Mount St. Helens dacite dome, 1980–1986, *in* Fink, J.H., ed., *Lava flows and domes, emplacement mechanisms and hazard implications*: Berlin, Springer, International Association of Volcanology and Chemistry of the Earth's Interior, *Proceedings in Volcanology*, v. 2, p. 3–24.
- Thornber, C.R., Pallister, J.S., Lowers, H.A., Rowe, M.C., Mandeville, C.W., and Meeker, G.P., 2007, Chemistry, mineralogy, and petrology of amphibole in Mount St. Helens 2004–2006 dacite, chap. 32 *in* Sherrod, D.R., Scott, W.E., and Stauffer, P.H., eds., *A volcano rekindled: the first year of renewed eruptions at Mount St. Helens, 2004–2006*: U.S. Geological Survey Professional Paper (this volume).
- Tuffen, H., Dingwell, D.B., and Pinkerton, H., 2003, Repeated fracture and healing of silicic magma generate flow banding and earthquakes?: *Geology*, v. 31, p. 1089–1092.
- Tuffen, H., and Dingwell, D., 2005, Fault textures in volcanic conduits: evidence for seismic trigger mechanisms during silicic eruptions: *Bulletin of Volcanology*, v. 67, p. 370–387.
- Turcotte, D.L., 1986, Fractals and fragmentation: *Journal of Geophysical Research*, v. 91, p. 1921–1926.
- Turcotte, D.L., 1992, *Fractals and chaos in geology and geophysics*: Cambridge, Cambridge University Press, 221 p.
- Vallance and others, 2007, Growth of recumbent dome and associated near-field deformation, chap. 9 *in* Sherrod, D.R., Scott, W.E., and Stauffer, P.H., eds., *A volcano rekindled: the first year of renewed eruption at Mount St. Helens, 2004–2006*: U.S. Geological Survey Professional Paper (this volume).
- Watts, R.B., Herd, R.A., Sparks, R.S.J., and Young, S.R., 2002, Growth patterns and emplacement of the andesite lava dome at Soufrière Hills Volcano, Montserrat: *Geological Society of London Memoir* 21, p. 115–152.
- Williams, H., 1932, The history and character of volcanic domes: University of California, *Bulletin of the Department of Geological Sciences*, v. 21, p. 51–146.
- Wilson, B., Dewers, T., Reches, Z., and Brune, J., 2005, Particle size and energetics of gouge from earthquake rupture zones: *Nature*, v. 434, p. 749–752.
- Wolf, K.J., and Eichelberger, J.C., 1997, Syneruptive mixing, degassing and crystallization at Redoubt Volcano, eruption of December 1989 to May, 1990: *Journal of Volcanology and Geothermal Research*, v. 75, p. 19–37.
- Wong, T.-f., David, C., and Zhu, W., 1997, The transition from brittle faulting to cataclastic flow in porous sandstones: mechanical deformation: *Journal of Geophysical Research*, v. 102, p. 3009–3025.
- Yund, R.A., Blanpied, M.L., Tullis, T.E., and Weeks, J.D., 1990, Amorphous material in high strain experiment fault gouge: *Journal of Geophysical Research*, v. 95, p. 15589–15602.